

# Verifying Operational Forecasts of Land-Sea Breeze and Boundary Layer

## Mixing Processes

Ewan Short\*

*School of Earth Sciences, and ARC Centre of Excellence for Climate Extremes, The University of  
Melbourne, Melbourne, Victoria, Australia.*

Ben ?. Price

*Bureau of Meteorology, Casuarina, Northern Territory, Australia*

Derryn ?. Griffiths and Alexei ?. Hider

*Bureau of Meteorology, Melbourne, Victoria, Australia*

\*Corresponding author address: School of Earth Sciences, The University of Melbourne, Melbourne, Victoria, Australia.

E-mail: shorte1@student.unimelb.edu.au

## ABSTRACT

13 Forecasts issued by the Australian Bureau of Meteorology are based on  
14 model data that is edited by human forecasters. Two types of edits are com-  
15 monly made to the wind fields: these aim to improve how boundary layer  
16 mixing processes and the land-sea breeze are resolved in the forecast. In this  
17 study we compare the diurnally varying component of the edited wind fore-  
18 cast, with those of station observations and unedited model guidance datasets,  
19 to assess the additional accuracy provided by the edits. We consider coastal  
20 locations across Australia over June, July and August 2018, assessing perfor-  
21 mance at three different spatial scales, and on both a daily and seasonal basis.  
22 The results show that the edited forecast generally only produces lower daily  
23 errors than model guidance at the coarsest spatial scale (1000 - 2000 km),  
24 but can achieve lower seasonal biases over all three spatial scales. However,  
25 the edited forecast only reduces errors at particular times and locations, and  
26 rarely produces lower errors than all model guidance products simultaneously.  
27 This suggests that forecaster skill lies mostly in making the choice of model  
28 guidance, rather than in making edits. To better diagnose the causes of er-  
29 rors in the diurnal wind cycles, we fit a modified ellipse to the climatological  
30 diurnal cycle hodographs. Performance varies with location for multiple rea-  
31 sons, including biases in the directions sea-breezes approach coastlines, am-  
32 plitude and shape biases in the hodographs, and disagreement as to whether  
33 sea-breeze or boundary layer mixing processes contribute most to the diurnal  
34 cycle.

## 35 1. Introduction

36 Modern weather forecasts are typically produced by models in conjunction with human fore-  
37 casters. Forecasters working for the Australian Bureau of Meteorology (BoM) construct a seven  
38 day forecast by loading model data into a software package called the Graphical Forecast Editor  
39 (GFE), then editing this model data using tools within the GFE. Is this also how things work at  
40 the U.S National Weather Service and U.K. Met Office? Forecasters can choose which model to  
41 base their forecast on, and refer to this as a choice of *model guidance*. Edits are typically made  
42 to account for processes that are under-resolved at synoptic scale model resolutions, or to correct  
43 known biases of the models being used. The resulting gridded forecast datasets are then provided  
44 to the public through the BoM's online MetEye data browser (Bureau of Meteorology 2019); the  
45 gridded forecast datasets are also translated into text and icon forecasts algorithmically.

46 Australian forecasters generally make two types of edits to the surface wind fields on a routine  
47 daily basis. The first is to edit the surface winds after sunrise at locations where the forecaster be-  
48 lieves the model guidance is providing a poor representation of boundary layer mixing processes.  
49 Boundary layer mixing occurs as the land surface heats up, producing an unstable boundary layer  
50 which transports momentum downward to the surface layer. Before this mixing occurs, winds  
51 are typically both weaker and ageostrophically oriented due to surface friction (Lee 2018), and so  
52 mixing can affect both the speed and direction of the surface winds. How do the boundary layer  
53 mixing tools in GFE currently work? While I was in Darwin you picked a height  $z$  and a percent-  
54 age  $p$ , and the tool essentially formed an average of the surface winds and winds at  $x$  weighted by  
55  $p$ .

56 The second type of edit involves changing the afternoon and evening surface winds around those  
57 coastlines where the forecaster believes the model guidance is resolving the sea-breeze poorly.

58 How do the sea-breeze tools in GFE currently work? While I was in Darwin you traced out the  
59 relevant coastline graphically, chose a wind speed and a time, and GFE would add in winds perpen-  
60 dicular to the traced coastline at this speed, and smoothly blend them in spatially and temporally.

61 Forecasters, and the weather services that employ them, have good reasons for ensuring the  
62 diurnally varying component of their wind forecasts are as accurate as possible. Dai and Deser  
63 (1999) fitted the first two harmonics to seasonal averages of wind speed at different times of day,  
64 and showed that over land surfaces the average amplitude of the wind speed diurnal cycle varied  
65 from 1.2 to 2.1 kn, (knots are used throughout this paper because this is the unit forecasters work  
66 with, and the unit that is used in Jive) and that the fitted harmonics accounted for 50 to 70% of  
67 the daily variability. Table 1 provides the mean wind speeds for the eight Australian capital city  
68 airport stations shown in Fig. 1, over December, January, February 2017/18, and June, July and  
69 August 2018, suggesting that the amplitude of the mean diurnal cycles are approximately 10 to  
70 34% of the mean wind speeds across Australia.

71 Beyond their contribution to the overall wind field, diurnal wind cycles are important for the  
72 ventilation of pollution, with sea-breezes transporting clean maritime air inland, where it helps  
73 flush polluted air out of the boundary layer (Miller et al. 2003; Physick and Abbs 1992). Further-  
74 more, diurnal wind cycles affect the function of wind turbines (Englberger and Dörnbrack 2018)  
75 and the design of wind farms (Abkar et al. 2016), as daily patterns of boundary layer stability  
76 affect turbine wake turbulence, and the losses in wind power that result.

77 To our knowledge, no published work has assessed the diurnal component of human edited  
78 forecasts, although some previous studies have assessed the performance of different operational  
79 models at specific locations. Svensson et al. (2011) examined thirty different operational model  
80 simulations, including models from most major forecasting centres utilising most commonly used  
81 boundary layer parametrisation schemes, and compared their performance with a large eddy sim-

82 ulation (LES), and observations at Kansas, USA, during October 1999. They found that both the  
83 models and LES failed to capture the sudden  $\approx 6$  kn jump in wind speeds shortly after sunrise, and  
84 underestimated morning low level turbulence and wind speeds. Other studies have assessed near-  
85 surface wind forecasts, verifying the total wind speeds, not just the diurnal component. Pinson  
86 and Hagedorn (2012) studied the 10 m wind speeds resolved by the European Centre for Medium  
87 Range Weather Forecasting (ECMWF) operational model ensemble across western Europe over  
88 December, January, February 2008/09. They found that the worst performing regions were coastal  
89 and mountainous areas, and attributed this to the small scale processes, e.g. sea and mountain  
90 breezes, that are under-resolved at ECMWF's coarse 50km spatial resolution.

91 Any attempt to validate model data against observations must confront the *representation prob-*  
92 *lem* (e.g. Zaron and Egbert 2006). Because models cannot resolve physical processes occurring  
93 at sub-grid scales, a value predicted by an operational model for a given grid-cell must be inter-  
94 preted as a prediction of the filtered, or Reynolds averaged value over that grid-cell. Therefore,  
95 comparing model data with observational data can be an unfair test of model performance, and for  
96 this reason model forecasts are often verified against reanalysis hind-casts that use the same model  
97 (e.g. Lynch et al. 2014).

98 However, the way the representation problem applies to the verification of forecasts issued to the  
99 public is more nuanced. In this case, a forecast issued by a national weather service is attempting  
100 to represent either reality itself, or the filtered version of reality *that is of interest to the end users*.  
101 Thus, Pinson and Hagedorn (2012) disregarded the representation problem entirely, arguing that  
102 the end user is not interested in spatiotemporal scales of models, only the “best forecast” at the  
103 time and place of their choice. However, different users will have different ideas about what  
104 the “best” forecast entails. Some users may desire a forecast that minimises error between the  
105 forecast and observations, others a forecast that most accurately reproduces the observed wind

106 speed distribution, regardless of temporal details. Ideally, operational forecasts should therefore  
107 be assessed according to the specific representation needs of particular end users.

108 Note that BoM verifies its wind forecasts by comparing hourly forecast data with station obser-  
109 vations that are first averaged 10 minutes either side of the hour: implicit in this practice is the  
110 assumption that end users do not care about wind turbulence at temporal scales less than 20 min-  
111 utes. Furthermore, the fact that the BoMs forecast is formed from model datasets with different  
112 resolutions, and the choice of model guidance can change even over the course of a single day,  
113 (e.g. Fig. 3 b), means it is difficult to determine precisely what BoM forecasts intend to represent,  
114 and hence addressing the representation problem is difficult. Note that clicking locations on the  
115 MetEye map seems to bring up the forecast for the nearest station or population centre. Does  
116 this imply that the Official forecast is intending to represent spatial scales at least as fine as the  
117 distance between stations? Or is it intending to represent averaged parameters at the ACCESS-R  
118 or ACCESS-C resolutions? Note also that grids are only provided every 3 hours in MetEye; do  
119 these grids represent the hourly values from the Official forecast, provided just at these three hour  
120 intervals, or a three hourly average?

121 Related to the representation problem is the question of how mesoscale models, which run at  
122 spatial resolutions of between 1 and 10 km, should be verified. BoM now regularly runs mesoscale  
123 models over some Australian capital cities as part of its daily forecasting routine, and the edits  
124 performed by human forecasters are also often mesoscale in nature. Note that mesoscale models  
125 resolve topography and its effects on the atmosphere in more detail, and explicitly simulate most  
126 convective and boundary layer processes. In this sense they are more realistic than coarser scale  
127 models, although they can actually perform worse than coarse models on standard verification  
128 scores whenever there are timing or location differences between features in the models and in  
129 observations. Mass et al. (2002) found that in the northwestern United States, mean square errors

130 in forecasts produced using mesoscale models decreased with resolution down to 10 to 15 km,  
131 whereas in the eastern United States where the topography is much flatter, this threshold was  
132 considerably larger, at 20 to 40 km.

133 Mass et al. (2002) therefore argued that existing verification approaches needed reform, suggest-  
134 ing that verification could instead be performed on spatially or temporally averaged parameters,  
135 an approach now known as *upsampling* (Ebert 2008). Alternatively, Mass et al. (2002) argued that  
136 “feature based” identification metrics be developed, which reward models for realistically simu-  
137 lating atmospheric features, even if the timing or location of these features is incorrect. Rife and  
138 Davis (2005) developed such a method for the verification of surface winds, defining a wind “ob-  
139 ject” as a wind change of at least one standard deviation occurring within a 12 hour interval, then  
140 assessing whether a mesoscale model could replicate the “objects” present in observations.

141 The present study has two goals. First, to describe a method for comparing the diurnal cycles  
142 of human edited wind forecasts to those of unedited model guidance forecasts, in order to assess  
143 where and when human edits produce an increase in accuracy, and to do so in a way that re-  
144 spects the representation and mesoscale verification challenges discussed above. Second, to apply  
145 this methodology across Australian coastal locations to better understand the performance of both  
146 boundary layer mixing and land-sea breeze forecaster edits. The remainder of this paper is organ-  
147 ised as follows. Section 2 describes the methodology and datasets to which it is applied, section 3  
148 provides results, and sections 4 and 5 provide a discussion and a conclusion, respectively.

## 149 **2. Data and Methods**

150 This study compares both human edited and unedited Australian Bureau of Meteorology (BoM)  
151 wind forecasts with automatic weather station (AWS) data across Australia. The comparison is

152 performed by first isolating the diurnal perturbations of each dataset, then comparing these pertur-  
153 bations on an hour-by-hour basis.

#### 154 *a. Data*

155 Four datasets are considered in this study; the human edited Official BoM wind forecast data that  
156 is issued to the public, observational data from automatic weather stations (AWS) across Australia,  
157 unedited model data from ECMWF, (is this the mean of the ECMWF operational ensemble?)  
158 and unedited model data from the Australian Community Climate and Earth System Simulator  
159 (ACCESS). ECMWF and ACCESS are two of the model guidance products most commonly used  
160 by Australian forecasters. (I haven't considered the BoM's Operational Consensus Forecast in this  
161 study, because it was not used in the Official forecast for winds while I was in the NT. If it is used  
162 frequently in other states, the study can be reinterpreted as a verification of both forecaster edits  
163 and OCF against unedited model guidance. Also, with the Bureau's permission, I would like to  
164 make the datasets used in this paper open access, and host them on, for instance, the NCI catalogue  
165 page.) The Official and ECMWF data are at ? and ? degree spatial resolutions respectively. What  
166 are the resolutions of these datasets as they're used in Jive? I know ACCESS uses nested grids,  
167 so what is the resolution of the ACCESS dataset when used in GFE and Jive? Are the outer  
168 grids interpolated to the resolution of the inner grids, or are the inner grids upscaled? Official,  
169 ACCESS and AWS data exists at each UTC hour, but ECMWF data only exists at a three hour  
170 resolution. Why is this? What are the actual time-steps of the models? To be consistent with the  
171 other data sets, ECMWF is therefore linearly interpolated to an hourly resolution: note that this  
172 is also what happens when forecasters load ECMWF wind data into the GFE, and the linearly-  
173 interpolated ECMWF data is therefore the appropriate model guidance dataset to compare with  
174 the Official forecast. To facilitate comparison with observations, Official, ACCESS and ECMWF



175 data is (tri-linearly?) interpolated in all three spatial dimensions to the locations of the weather  
176 stations. AWS wind data is recorded every minute at each station, and the hourly AWS datasets  
177 used in this study are formed by taking 10 minute averages either side of each UTC hour. (My  
178 memory is that Jive uses a ten minute average either side, but need to confirm this as it could  
179 be five minutes either side.) Stations are quality controlled by... I've excluded the list of known  
180 problematic wind stations in the Jive documentation, but I can't remember what the other quality  
181 control methods were.

182 Both ACCESS and ECMWF use parametrisation schemes to simulate sub-grid scale boundary  
183 layer turbulence, and the resultant mixing. ACCESS uses the schemes of Lock et al. (2000) and  
184 Louis (1979) for unstable and stable boundary layers respectively (Bureau of Meteorology 2010).  
185 ECMWF use similar schemes that they develop in-house (European Center for Medium Range  
186 Weather Forecasting 2018). This study considers the austral winter months of June, July and  
187 August 2018. This short time period was chosen to reduce the effect of changing seasonal and  
188 climatic conditions, changing forecasting practice and staff, and of developments to the ACCESS  
189 and ECMWF models.

## 190 *b. Assessing Diurnal Cycles*

191 Forecasters typically edit model guidance wind data to account for under-resolved sea-breezes  
192 and boundary layer mixing processes. Instead of attempting to assess each type of edit individually,  
193 we study the overall diurnal signal by subtracting a twenty hour centred running mean *background*  
194 *wind* from each zonal and meridional hourly wind data point. This provides a collection of zonal  
195 and meridional wind *perturbation* datasets.

196 One measure of the accuracy of the Official, ACCESS and ECMWF diurnal cycles is to com-  
197 pare the Euclidean distances of the perturbations at each hour with the corresponding AWS per-

198 turbations. For example, to assess whether the Official forecast perturbations,  $\mathbf{u}_O$ , or ACCESS  
 199 perturbations,  $\mathbf{u}_A$ , best match the AWS observations,  $\mathbf{u}_{AWS}$ , we calculate the *Wind Perturbation*  
 200 *Index* (WPI), defined by

$$\text{WPI}_{OA} = |\mathbf{u}_{AWS} - \mathbf{u}_A| - |\mathbf{u}_{AWS} - \mathbf{u}_O|. \quad (1)$$

201 The analogously defined quantities  $\text{WPI}_{OE}$  and  $\text{WPI}_{EA}$  can then be used to provide a comparison  
 202 of the Official and ECMWF perturbations, and of the ACCESS and ECMWF perturbations, re-  
 203 spectively. We can then take means of the WPI on an hourly basis; i.e. all the 00:00 UTC WPI  
 204 values are averaged, all the 01:00 UTC values are averaged, and so forth, and denote such an  
 205 average by  $\overline{\text{WPI}}$ .

206  $\overline{\text{WPI}}$  is the difference of two mean absolute errors. A  $\overline{\text{WPI}}_{OA}$  value of 0.5 kn at 00:00 UTC  
 207 means that the Official 00:00 UTC perturbations are, on average, 0.5 kn closer to the observed  
 208 perturbations than are those of ACCESS. The WPI compares just *one aspect* of the Official forecast  
 209 with model guidance; it says nothing, for instance, about whether the variability of the Official  
 210 forecast is closer to that of the AWS than the model guidance. As such, any statements about  
 211 performance made throughout this paper refer solely to WPI, and no claim is being made that WPI  
 212 is sufficient to completely characterise the accuracy, or value to the user, of how the surface diurnal  
 213 wind cycle is represented in competing forecasts.

214 Note that sea-breeze and boundary layer mixing processes depend crucially on the background  
 215 atmospheric conditions in which they occur. By comparing wind perturbations rather than the  
 216 overall wind fields we are not claiming these background conditions are irrelevant. However,  
 217 when a forecaster makes an edit of a wind forecast to better resolve these processes, they are  
 218 implicitly assuming that future background conditions will be close enough to either climatology,  
 219 or model predictions of background conditions, to justify making the edit. Thus, it makes sense to

220 compare forecast perturbations to observed perturbations, as long as errors are interpreted as the  
221 consequence not only of how the forecaster or model resolves the diurnal cycle, but of how errors  
222 in the background state contribute to errors in the perturbations. To minimise the significance of  
223 background state errors, this study focuses exclusively on lead-day one forecasts.

224 Given the large degree of turbulence and unpredictable variability in both the AWS, Official,  
225 and model datasets, care must be taken to ensure we do not pre-emptively conclude Official has  
226 outperformed the model guidance when  $\overline{\text{WPI}} > 0$  purely by chance. The method for estimating  
227 confidence in  $\overline{\text{WPI}}$  is based on a method proposed by Griffiths et al. (2017) as a general frame-  
228 work for BoM verification metrics. Note first that WPI is defined so as to minimise the temporal  
229 autocorrelations within each dataset, and to avoid having to consider correlations between the  
230 zonal and meridional components within and between datasets. Time series formed from the WPI  
231 values at a particular time, say 00:00 UTC, across the three month time period, can therefore be  
232 idealised as an independent random sample of a random variable  $W$ . The sampling distribution for  
233 each  $\overline{\text{WPI}}$  can be modelled by a Student's  $t$ -distribution, and from this we calculate the probability  
234 that  $W$  is positive, denoted  $\Pr(W > 0)$ . Although temporal autocorrelations of WPI, i.e. corre-  
235 lations between WPI values at a particular hour from one day to the next, are in practice small  
236 or non-existent thanks to how WPI is defined, they are still accounted for by reducing the “ef-  
237 fective” sample size to  $n(1 - \rho_1) / (1 + \rho_1)$ , where  $n$  is the actual sample size and  $\rho_1$  is the lag-1  
238 autocorrelation (Zwiers and von Storch 1995; Wilks 2011). Note that in the standard language of  
239 statistical hypothesis testing, we would reject the null hypothesis that  $W = 0$  at significance level  
240  $\alpha$  if  $\Pr(W > 0) > 1 - \frac{\alpha}{2}$  or  $\Pr(W < 0) > 1 - \frac{\alpha}{2}$ . However, in this study we are interested in both  
241 whether  $W > 0$  or whether  $W < 0$ , so prefer to simply state the value of  $\Pr(W > 0)$ , referring to  
242 this as a *confidence score*, and noting  $\Pr(W < 0) = 1 - \Pr(W > 0)$ . We say Official outperforms  
243 model guidance with “high confidence” if  $\Pr(W > 0) \geq 95\%$ , or that model guidance outperforms

244 Official with “high confidence” if  $\Pr(W > 0) \leq 5\%$ , with high confidence implicit whenever it is  
245 not explicitly mentioned. Much of this explanation is probably unnecessary, but would like to get  
246 feedback before I trim it.

247 To investigate the consequences of the representation and mesoscale verification challenges dis-  
248 cussed in section 1, we apply *upsampling* (Ebert 2008), where forecast and observational data are  
249 first averaged to coarser spatiotemporal scales before being compared. In this study we consider  
250 three spatial and two temporal scales. The finest spatial scale is that of the individual station.  
251 This study focuses on the 8 capital city airport stations, marked by stars in Fig. 1, as their high  
252 operational significance means that they are typically the most accurate and well maintained. The  
253 next spatial scale is formed by taking the 10 stations closest to each capital city airport station,  
254 with some flexibility allowed to ensure stations are roughly parallel to the nearest coastline. These  
255 station groups are referred to as the *airport station groups*. The coarsest spatial scale is formed by  
256 taking all stations within 150 km of the nearest coastline, and grouping these by state. This is done  
257 because Australian forecasts are currently produced on a state by state basis at forecasting centres  
258 based in each state capital, with each forecasting centre utilising different forecasting practices.  
259 Indeed, the Official gridded forecast typically shows slight discontinuities across state boundaries  
260 (Bureau of Meteorology 2019). Note that the Western Australian coastline is subdivided into three  
261 pieces, and stations along the Gulf of Carpentaria, north Queensland Peninsula, and Tasmanian  
262 coastlines are neglected, in order to ensure each station group corresponds to an approximately  
263 linear segment of coastline, so as to best resolve the land-sea breeze signal after spatial averaging  
264 (e.g. Vincent and Lane 2016). These eight station groups are referred to as the *coastal station*  
265 *groups*.

266 We also consider both daily and seasonal time scales. For daily time scales, we either consider  
267 just the individual airport stations, or modify the definition of WPI in equation (1) so that each

268 perturbation dataset is first spatially averaged over either the airport or coastal station groups.  
 269 Confidence scores are calculated for the airport and coastal station groups in the same way as for  
 270 the single airport stations, treating the spatially averaged data as a single time series. This provides  
 271 a conservative way to deal with spatial correlation between the stations in each group (Griffiths  
 272 et al. 2017).

273 For the seasonal scale comparison we define the *Climatological Wind Perturbation Index*  
 274 (CWPI) by

$$\text{CWPI}_{\text{OA}} = |\overline{\mathbf{u}}_{\text{AWS}} - \overline{\mathbf{u}}_{\text{O}}| - |\overline{\mathbf{u}}_{\text{AWS}} - \overline{\mathbf{u}}_{\text{A}}|, \quad (2)$$

275 where the over-bars denote temporal averages of the perturbations at a particular hour, across the  
 276 three month time period. These temporally averaged perturbations represent the climatological  
 277 diurnal wind cycle over the three month study period for each dataset.  $\text{CWPI}_{\text{OE}}$  and  $\text{CWPI}_{\text{EA}}$  are  
 278 defined analogously. The three spatial scales are considered in the same way as for WPI, with the  
 279 spatial average taken before the temporal average. Uncertainty in the CWPI is estimated through  
 280 bootstrapping (Efron 1979). This is done by performing resampling with replacement on the  
 281 underlying perturbation datasets, and calculating the CWPI multiple times using these resampled  
 282 datasets. This provides a distribution of CWPI values, which analogously to with WPI, we treat as  
 283 a sample from a random variable  $C$ , and use this to estimate  $\text{Pr}(C > 0)$ .

284 Although the WPI and CWPI provide quantitative information on the accuracy of the diurnal cycle  
 285 at different times of day, they do not provide much information on the structure of the diurnal wind  
 286 cycles of each dataset. Gille et al. (2005) obtained summary statistics on the observed structure of  
 287 the climatological diurnal wind cycles across the globe by using linear regression to calculate the

288 coefficients  $u_i, v_i$   $i = 0, 1, 2$ , for the fits

$$u = u_0 + u_1 \cos(\omega t) + u_2 \sin(\omega t), \quad (3)$$

$$v = v_0 + v_1 \sin(\omega t) + v_2 \sin(\omega t), \quad (4)$$

289 where  $\omega$  is the angular frequency of the earth and  $t$  is the local solar time in seconds. These  
 290 fits trace out ellipses in the  $x, y$  plane, and descriptive metrics, like the eccentricity of the ellipse,  
 291 and the angle the semi-major axis makes with the horizontal, can be calculated directly from the  
 292 coefficients  $u_1, u_2, v_1$  and  $v_2$ . Gille et al. (2005) applied this fit to scatterometer data, which after  
 293 temporal averaging resulted in just four zonal and meridional values per location, and as such the  
 294 fit performed very well.

295 However, equations (3) and (4) do not provide a good fit for hourly wind data, primarily because  
 296 they assume a twelve hour symmetry in the evolution of the diurnal cycle. In practice, asymmetries  
 297 between daytime heating and nighttime cooling (e.g. Svensson et al. 2011) result in surface wind  
 298 perturbations accelerating rapidly just after sunrise, but remaining comparatively stagnant at night  
 299 (e.g. Fig. 9). Thus, we instead fit the equations

$$u = u_0 + u_1 \cos(\alpha(\psi, t)) + u_2 \sin(\alpha(\psi, t)), \quad (5)$$

$$v = v_0 + v_1 \sin(\alpha(\psi, t)) + v_2 \sin(\alpha(\psi, t)), \quad (6)$$

300 to the climatological perturbations, with  $\alpha$  the function from  $[0, 24) \times [0, 2\pi) \rightarrow [0, 2\pi)$  given by

$$\alpha(\psi, t) \equiv \pi \left[ \sin \left( \pi \frac{(t - \psi) \bmod 24}{24} - \frac{\pi}{2} \right) + 1 \right], \quad (7)$$

301 with  $t$  the time in units of hours UTC, and  $\psi$  providing the time when the wind perturbations vary  
 302 least with time. For each climatological diurnal wind cycle, we solve for the seven parameters  $u_0$ ,  
 303  $u_1, u_2, v_0, v_1, v_2$  and  $\psi$  using nonlinear regression, performed using the `least_squares` function  
 304 from the `scipy.optimize` python module (SciPy 2019).

Note Gille et al. (2005) fit equations (3) and (4) to the temporally averaged wind fields, so that  $(u_0, v_0)$  could be interpreted as the mean wind over the study's time period, and the remaining terms providing the climatological diurnal perturbations. In this study we fit equations (5) and (6) to the climatological perturbations themselves, with  $(u_0, v_0)$  now necessary to offset the asymmetry introduced by  $\alpha$ , i.e. to ensure the time integral of the fitted perturbation values is approximately zero. Following Gille et al. (2005), the ellipse's orientation, i.e. the angle the semi-major axis of the ellipse makes with lines of latitude, as well as the ellipse's eccentricity are calculated algebraically, but the perturbation speed maximum, and the time at which this maximum is achieved, are instead obtained numerically.

### 3. Results

In this section, the methods described in section 2 are applied to Australian forecast and station data over the months of June, July and August (austral winter) 2018. First, absolute errors are compared on a daily basis using the Wind Perturbation Index (WPI) at three different spatial scales. Second, overall seasonal biases during this time period are assessed using the Climatological Wind Perturbation Index (CWPI), and by comparing structural indices derived from ellipses fitted to the climatological wind perturbations.

#### *a. Daily Comparison*

Figure 2 provides the WPI values and confidence scores for the coastal station groups for  $\overline{\text{WPI}}_{\text{OA}}$ ,  $\overline{\text{WPI}}_{\text{OE}}$  and  $\overline{\text{WPI}}_{\text{EA}}$ , which represent the the Official versus ACCESS, Official versus ECMWF, and ECMWF versus ACCESS comparisons, respectively. The results indicate that for the majority of station groups and hours, both the unedited ACCESS and ECMWF models outperform the Official forecast. The lowest  $\overline{\text{WPI}}$  values occur at the NT station group at 23:00 and 00:00 UTC

for both  $\overline{\text{WPI}}_{\text{OA}}$  and  $\overline{\text{WPI}}_{\text{OE}}$ . Although Official outperforms at least one of ACCESS or ECMWF at multiple times and station groups, the only group and time where it outperforms both is 05:00 UTC over the South WA station group, although the  $\overline{\text{WPI}}$  values are comparatively low. ECMWF generally outperforms ACCESS from 10:00 - 14:00 UTC, with the South WA station group being the main exception.

Figures 3 and 4 provide case studies of the NT and South WA station groups, respectively. Figure 3 a) provides a time series of WPI for the NT station group at 23:00 UTC. The time series shows significant temporal variability, with WPI frequently dropping below  $-2$  kn. Figures 3 b) and c) show hodographs of the winds and wind perturbations, respectively, for the AWS observations, Official forecast, and ACCESS and ECMWF model datasets, at each hour UTC on the 3<sup>rd</sup> of July, which provides an interesting example.

Figure 3 b) shows that the Official wind forecast on this day was likely based on edited ACCESS from 00:00 to 06:00 UTC, then edited ECMWF from 07:00 to 13:00 UTC, then unedited ACCESS from 15:00 to 21:00 UTC. The final two hours of the forecast show the Official winds acquiring a stronger east-northeasterly component than the other datasets. This rapid change is clearer in the perturbation hodograph shown in Fig. 3 c). At this time of year the prevailing winds throughout the NT are east-southeasterly, and 22:00 UTC corresponds to  $\approx 08:30$  local solar time (LST) in this region, so the rapid departure of the Official forecast from ACCESS at this time likely represents an edit made by a forecaster to capture boundary layer mixing processes.

Figure 5 a) shows the first ten values from wind soundings at Darwin Airport at 12:00 UTC on July 3<sup>rd</sup> and 00:00 UTC on July 4<sup>th</sup>. In both instances the winds are indeed east-southeasterly, and so the rapidly changing wind perturbations at 22:00 UTC in the Official forecast likely reflect a boundary layer mixing edit that has been applied either too early, or has strengthened the south-



350 easterly component of the winds too much. Similar issues create low WPI scores on the 8<sup>th</sup> of  
351 June and 9<sup>th</sup> and 10<sup>th</sup> of July.

352 Figure 4 a) provides a time series of WPI for the South WA station group at 05:00 UTC. As with  
353 the NT station group there is significant temporal variability, with WPI frequently exceeding 1 kn.  
354 Figures 4 b) and c) provide hodographs of the winds and wind perturbations, respectively, on the  
355 9<sup>th</sup> of June, which is an interesting example. The perturbation hodograph shows both ECMWF  
356 and ACCESS under-predicting the amplitude of the diurnal wind cycle on this day. In each dataset  
357 the 05:00 UTC perturbations are westerly to northwesterly, and given the orientation of the South  
358 WA coastline (see Fig. 1) and the fact that 05:00 UTC corresponds to around 13:00 local solar  
359 time (LST) in this region, the perturbations likely indicate boundary layer mixing processes.

360 Figure 5 shows wind soundings at Perth Airport, the nearest station to the South WA station  
361 group to provide wind soundings, between 12:00 UTC on the 8<sup>th</sup> June and 12:00 UTC on the 9<sup>th</sup>  
362 June. The 8<sup>th</sup> June 12:00 UTC sounding shows surface northerlies of around 6 kn, becoming west  
363 to northwesterlies of over 20 kn 2.4 km above the surface. However, the subsequent sounding at  
364 00:00 UTC on the 9<sup>th</sup> of June shows that the winds acquire a strong northerly component of 30  
365 kn in the first 500 m of the atmosphere, with the final sounding indicating a strong northwesterly  
366 wind at 725 m persisting until 12:00 UTC. In Fig. 4 c), the Official perturbations from 04:00 to  
367 07:00 UTC show stronger westerly perturbations than either ACCESS or ECMWF, improving the  
368 amplitude of Official's diurnal wind cycle. However, the AWS perturbations are more northerly  
369 than those of Official, and so the Official forecast winds have been strengthened in a slightly  
370 incorrect direction. One explanation for this discrepancy is that the Official forecast has been  
371 edited based on the June 8<sup>th</sup> 12:00 UTC sounding, with the winds above the surface changing  
372 direction in the subsequent 12 hours. A similar explanation can be given for the high WPI scores on

the 3<sup>rd</sup> of August, although in this case the Official forecast slightly improves both the magnitude and direction of the 05:00 UTC wind perturbations.

To contrast with the coastal station group results, Fig. 6 presents the  $\overline{WPI}$  values and confidence scores for  $\overline{WPI}_{OE}$ , which represents the Official versus ECMWF comparison, for the airport stations, and airport station groups. The results for the airport stations are noisier than the results for the coastal station groups in Figs. 2 c) and d), although they share some similarities. Official outperforms ECMWF at 01:00 and 02:00 UTC at both the Darwin airport station and the NT station group, although ECMWF outperforms Official between 08:00 and 14:00 UTC at Darwin and Brisbane airports, and the corresponding NT and QLD station groups, with the exception of the QLD station group at 12:00 UTC. ECMWF also outperforms Official at Hobart airport at almost all hours of the day, and at Adelaide and Canberra airports from 11:00 to 14:00 UTC.

For the remaining stations and times, Official only outperforms ECMWF at the Perth airport station at 06:00 UTC and the Melbourne airport station at 01:00 UTC, although in both cases WPI values are comparatively small in magnitude. Furthermore, in both cases there is no clear pattern to the  $\overline{WPI}_{OE}$  values over the rest of the day. Note that the *multiplicity problem* (Wilks 2011, p. 178) requires care be taken before giving meaning to these two examples: i.e., given that we are calculating twenty four confidence scores for eight stations, then if WPI were uncorrelated across each station and hour we would expect to find  $0.05 \times 24 \times 8 \approx 10$  instances where  $P(W_{OE} > 0) \geq 95\%$ , even if  $W_{OE}$  were in fact equal to zero.

For the airport station groups, ECMWF outperforms Official for the majority of station groups and times. The main exception is the Darwin airport station group, where Official outperforms ECMWF at 02:00 UTC, and there is ambiguity as to whether Official or ECMWF performs better at 01:00, 03:00 and 04:00 UTC, and from 15:00 to 22:00 UTC. In the analogous  $\overline{WPI}_{OA}$  Official versus ACCESS comparisons (not shown), the airport station results are similarly noisy, although

the airport station group results are slightly more favourable to Official, with Official outperforming ACCESS from 10:00 to 12:00 UTC at the Brisbane station group, and fewer occasions overall where ACCESS outperforms Official than ECMWF does.

Figure 7 presents the  $\overline{\text{WPI}}$  values and confidence scores for  $\overline{\text{WPI}}_{\text{EA}}$ , which represents the ECMWF versus ACCESS comparison, for the airport stations, and airport station groups. As with the Official versus ECMWF comparison in Fig. 6, the results for the airport stations are noisy, but more often than not show that ECMWF outperforms ACCESS. The results for the airport station group show ECMWF usually outperforms ACCESS, the main exceptions being the Darwin and Canberra airport station groups. Might be interesting to note that ACCESS-C+ does not run over Darwin or Canberra, possibly explaining the better performance of ACCESS there.

Naively, the fact that ECMWF generally outperforms ACCESS at these scales is surprising, as ACCESS runs at a higher spatiotemporal resolution than ECMWF, and is calibrated for Australian conditions. However, these results are not surprising in light of the mesoscale verification challenges discussed in section 1. The AWS data resolves motion with time scales as low as 10 minutes, and at arbitrarily small spatial scales: it therefore includes more unpredictable turbulence than either model dataset. Furthermore, because ACCESS runs at higher spatiotemporal resolutions than ECMWF, it includes additional scales of motion, and therefore adds additional variability to the wind fields. Unless the additional variability in ACCESS is perfectly correlated with observations, the average of  $|\mathbf{u}_{\text{AWS}} - \mathbf{u}_{\text{A}}|$  will therefore increase, unless this additional variability is compensated for by a reduction in bias, i.e.  $|\overline{\mathbf{u}}_{\text{AWS}} - \overline{\mathbf{u}}_{\text{A}}|$  decreases. These ideas are discussed in greater detail in section 4. Note finally that the results for the Official versus ECMWF comparison in Fig. 6 largely mirror those of the ECMWF versus ACCESS comparison in Fig. 7, suggesting that similar arguments apply to Official, as it is based on both ACCESS and ECMWF, as well as forecaster edits, which contribute additional variability.

## *b. Seasonal Comparison*

Figure 8 provides the Climatological Wind Perturbation Index (CWPI) values and confidence scores for the coastal station groups for  $CWPI_{OA}$ ,  $CWPI_{OE}$  and  $CWPI_{EA}$ , which represent the Official versus ACCESS, Official versus ECMWF, and ECMWF versus ACCESS comparisons, respectively. At the NT station group Official outperforms both ACCESS and ECMWF at 03:00 UTC with confidence  $\geq 93\%$ . However, both ACCESS and ECMWF outperform Official at 23:00 and 00:00 UTC, consistent with the  $\overline{WPI}$  results of Fig. 2. The NT station group results are discussed in more detail in section 4.

At the North WA station group at 01:00, 03:00 and 04:00, Official outperforms ACCESS with confidence scores of 77, 78 and 90%, respectively; Official also outperforms ECMWF at 01:00 and 02:00 UTC with confidence scores above 99%. Figure 9 a) shows that ECMWF's poor performance at 01:00 and 02:00 UTC is simply due to its linear interpolation at these times, whereas Official's very slight outperformance of ACCESS at 01:00, 03:00 and 04:00 is due to ACCESS's climatological diurnal cycle being slightly out of phase with that of the AWS observations, and the Official forecast correcting for this somewhat. Both Official and ECMWF slightly exaggerate the magnitude of the climatological sea-breeze, which peaks around 09:00 UTC, with ACCESS performing well in this respect.

At the South WA station group from 01:00 to 05:00 UTC, Official outperforms ECMWF with confidence scores of at least 88%. Figure 9 b) shows that ECMWF underestimates the westerly perturbations at these times, with these perturbations likely associated with boundary layer mixing processes, as discussed in section 3 a. Each of Official, ACCESS and ECMWF noticeably underestimate the amplitude of the diurnal cycle between 02:00 and 10:00 UTC, including both the westerly perturbations and the southerly sea-breeze perturbations.

444 At the NSW station group from 17:00 to 19:00 UTC, Official outperforms both ACCESS and  
445 ECMWF with confidence scores of at least 95% and 75%, respectively. Figure 9 c) shows  
446 that these times correspond to “dimples” in the perturbation hodographs that are present in all four  
447 datasets. The Official hodograph closely resembles that of ACCESS, except for this dimple, which  
448 has been exaggerated relative to ACCESS. **Don’t know what is going on here.** Figure 9 c) also  
449 shows that although ECMWF exaggerates the amplitude of the easterly sea-breeze perturbations,  
450 it captures the narrower shape of the AWS hodograph better than Official or ACCESS.

451 At the SA station group from 02:00 to 05:00 UTC and 09:00 to 12:00 UTC, Official outperforms  
452 both ACCESS and ECMWF, although confidence scores do not exceed 88% and 65% respectively.  
453 Figure 9 d) shows that although the Official forecast captures the amplitude of the perturbations  
454 from 01:00 to 05:00 UTC almost perfectly, its diurnal cycle is out of phase with that of the AWS  
455 during this period, explaining why Official only slightly outperforms ACCESS in the results of  
456 Figures 8 a) and b).

457 For contrast, Fig. 10 presents the CWPI values and confidence scores for  $CWPI_{OE}$ , which  
458 represents the Official versus ECMWF comparison, for the airport stations, and airport station  
459 groups. These results show much greater similarity with the Official versus ECMWF comparisons  
460 at the coastal station groups shown in Figs. 8 c) and d), than do the analogous  $\overline{WPI}$  results in  
461 Fig. 6 and Figs. 2 c) and d). This likely because the temporal averaging has reduced the addi-  
462 tional unpredictable variability in Official, revealing biases in Official and ECMWF that are partly  
463 shared across the three spatial scales. This point is discussed further in section 4. The analogous  
464 CWPI comparisons with ACCESS (not shown) are more ambiguous, although are generally more  
465 favourable for Official than those for  $\overline{WPI}$ . For example Official outperforms both ACCESS and  
466 ECMWF at Darwin Airport from 02:00 to 03:00 and 15:00 to 17:00 UTC with at least 90% confi-  
467 dence. However, Official performs less well compared to ACCESS over the airport station groups,

468 with CWPI values close to zero for most times and station groups, but ACCESS now strongly  
469 outperforming Official over the Darwin Airport station group.

470 Note that the hodographs in Fig. 9 are roughly elliptical in shape, suggesting that descriptive  
471 quantities can be estimated by fitting equations (5) and (6) to the zonal and meridional climato-  
472 logical perturbations, as described in section 2. Figure 11 provides the  $R^2$  values for the fits of  
473 the zonal and meridional perturbations to equations (5) and (6), respectively. The fit performs best  
474 at the coastal station group spatial scale, with  $R^2$  generally above 95%. It also performs well at  
475 the airport station and airport station group scales, with a few exceptions, including the ACCESS  
476 and Official meridional perturbations at the Canberra airport station group, and the ECMWF zonal  
477 perturbations at Melbourne airport.

478 The ellipse fits are used to derive four descriptive quantities: the maximum perturbation speed,  
479 the eccentricity of the fitted ellipse, the angle the fitted ellipse's semi-major axis makes with lines  
480 of latitude, and the time maximum perturbation speed occurs. Figure 12 provides these four quan-  
481 tities for each dataset and location across the three spatial scales. A variety of structural differences  
482 are apparent at a number of locations and scales. For example, Fig. 12 a) shows that at Brisbane air-  
483 port, the maximum AWS perturbation is at least 1 kn greater than Official, ACCESS and ECMWF,  
484 and Fig. 12 c) shows that the orientation of the AWS fitted ellipse is at least 20 degrees anti-  
485 clockwise from the other datasets. Figures 13 a) and b) show hodographs of the Brisbane airport  
486 perturbation climatology and ellipse fit, respectively. Although the ellipse fits suppress some of the  
487 asymmetric details, they capture the amplitudes and orientations of the real climatological diurnal  
488 cycles well. In this case the results show that the average AWS sea-breeze approaches from the  
489 northeast, whereas the Official, ECMWF and ACCESS sea-breezes approach more from the east-  
490 northeast. To check whether this just represents a direction bias of the Brisbane Airport station,  
491 Fig. 12 shows the climatological perturbations at the nearby Spitfire Channel station (see Fig. 1

492 for the location of this station, and other stations referred to in this section). While the amplitude  
493 bias is smaller at Spitfire Channel than Brisbane Airport, the directional bias is at least as high.  
494 A similar directional bias is evident at the nearby Inner Beacon station (not shown), although the  
495 bias is smaller than at Spitfire Channel and Brisbane Airport. Thus, the directional bias in Official,  
496 ACCESS and ECMWF at these stations is likely genuine, and not just a consequence of biased  
497 AWS observations. Figure 1 shows there are two small islands to the east of Brisbane airport; the  
498 more northwesterly orientation of the Brisbane Airport sea-breeze suggests these islands may be  
499 redirecting winds between the east coast of Brisbane and the west coasts of these islands, and that  
500 this local effect is not being captured in Official, ACCESS or ECMWF.

501 Another example is the Hobart Airport station. Figure 12 c) shows that the ellipse fits for the  
502 AWS perturbations are oriented 31, 35 and 62 degrees anti-clockwise from the ECMWF, Official  
503 and ACCESS ellipse fits, respectively. Figures 11 a) and b) show that the ellipse fit for the AWS  
504 perturbations at Hobart airport only achieve  $R^2$  values of 59% and 68% for the  $u$  and  $v$  components,  
505 respectively. However, figures 13 d) and e) show that the fit still captures orientations accurately,  
506 although it underestimates the maximum AWS perturbation. Figure 13 f) shows the climatological  
507 perturbations at the Hobart (city) station, which also show a large difference in orientation between  
508 ACCESS and AWS. Given the timing of the westerly perturbations in ACCESS, and the fact  
509 that the prevailing winds around Tasmania are westerly, these results suggest that ACCESS is  
510 exaggerating the boundary layer mixing processes involved in the diurnal cycle around Hobart.

511 The South WA station group also provides an interesting example. Here the ACCESS and  
512 Official ellipse fits are oriented at least 49 degrees anti-clockwise from those of AWS and ECMWF,  
513 and the ECMWF perturbations peak between 1.2 and 2.5 hours after the other datasets. These  
514 differences occur because eccentricity values are low for this station group, and Figure 9 b) shows  
515 that the westerly perturbations associated with boundary layer mixing are weaker for ECMWF

516 that the other datasets. A similar issue affects the VIC station group, explaining why the AWS  
517 ellipse fit is oriented at least 49 degrees anti-clockwise from those of the other datasets.

518 The Darwin Airport, Darwin Airport station group, and NT station group provide further exam-  
519 ples. In these cases there are timing differences between the perturbation maximums of up to 8.2  
520 hours. Figure 14 shows that these differences occur because for some datasets, the later north to  
521 northwesterly sea-breeze perturbations dominate the diurnal wind cycle, but for other datasets the  
522 earlier easterly to southeasterly boundary layer mixing effects dominate.

#### 523 4. Discussion

524 The results of section 3 may have implications for forecasting practice. If the goal of land-sea  
525 breeze and boundary layer mixing edits is to reduce absolute errors in the following day’s forecast  
526 of the surface wind fields, then a necessary (but not sufficient) condition for this to occur is for  
527 these edits to at least reduce the absolute errors in the diurnal component of the surface wind fields.  
528 However, the WPI comparisons in Figs. 2 and 6 suggest that this is only possible when absolute  
529 error is calculated at coarse spatial scales. If the Official forecast is based, at least partly, on an  
530 edited high resolution model guidance dataset like ACCESS, then due to the mesoscale verification  
531 issues discussed in section 1, the larger absolute errors associated with a higher resolution model  
532 completely mask the effect of the edits, with a lower resolution unedited model like ECMWF  
533 scoring better overall. While the CWPI results in Figs. 8 and 6 suggest that forecaster edits can  
534 improve the accuracy of diurnal wind cycles in a climatological sense, it is not clear if these  
535 improvements have operational significance.

536 To investigate these ideas further, consider first just the zonal components of the AWS and  
537 Official wind perturbations, denoted by  $u_{\text{AWS}}$  and  $u_{\text{O}}$  respectively. Considering just the values at  
538 a particular hour UTC, at a particular station, over the entire June, July, August time period, the



mean square error  $\text{mse}(u_{\text{AWS}}, u_{\text{O}}) = \overline{(u_{\text{AWS}} - u_{\text{O}})^2}$  can be decomposed

$$\text{mse}(u_{\text{AWS}}, u_{\text{O}}) = \underbrace{\text{var}(u_{\text{AWS}}) + \text{var}(u_{\text{O}}) - 2 \cdot \text{covar}(u_{\text{AWS}}, u_{\text{O}})}_{\text{var}(u_{\text{AWS}} - u_{\text{O}})} + \underbrace{(\bar{u}_{\text{AWS}} - \bar{u}_{\text{O}})^2}_{\text{squared bias}} \quad (8)$$

where  $\text{var}$ ,  $\text{covar}$  and over-bars denote the sample variance, covariance and mean respectively. The first three terms are the total variance of  $u_{\text{AWS}} - u_{\text{O}}$ , whereas the last term is the square of the bias between  $u_{\text{AWS}}$  and  $u_{\text{O}}$ . Note that the mean square error  $\text{mse}(u_{\text{AWS}}, u_{\text{O}})$  is closely related to  $\overline{\text{WPI}}$ , which is the difference between the mean absolute error of Official and AWS, and a model guidance dataset and AWS. Similarly, the CWPI is closely related to the squared bias component  $(\bar{u}_{\text{AWS}} - \bar{u}_{\text{O}})^2$  of the mean square error. Equation (8) can also be applied to wind perturbations that have first been spatially averaged over a station group, and to  $\text{mse}(u_{\text{AWS}}, u_{\text{E}})$  and  $\text{mse}(u_{\text{AWS}}, u_{\text{A}})$ , where  $u_{\text{E}}$  and  $u_{\text{A}}$  are the ECMWF and ACCESS zonal perturbations, respectively.

Figure 15 shows each term in the mean square error decomposition of equation 8 for both  $\text{mse}(u_{\text{AWS}}, u_{\text{O}})$  and  $\text{mse}(u_{\text{AWS}}, u_{\text{E}})$ , for Darwin Airport, the Darwin station group, and the NT station group. This region provides an interesting case study because Fig. 6 shows that Official has some skill at both Darwin Airport and over Darwin Airport station groups, in contrast to most other locations. At Darwin Airport,  $\text{mse}(u_{\text{AWS}}, u_{\text{O}})$  exceeds  $\text{mse}(u_{\text{AWS}}, u_{\text{E}})$  from 04:00 to 16:00 UTC due to higher total variance, whereas outside of these times  $\text{mse}(u_{\text{AWS}}, u_{\text{E}})$  exceeds  $\text{mse}(u_{\text{AWS}}, u_{\text{O}})$  due to larger bias. The higher total variance of  $u_{\text{AWS}} - u_{\text{O}}$  occurs because  $\text{var}(u_{\text{O}}) > \text{var}(u_{\text{E}})$ . This additional variability is mostly random from 04:00 to 14:00 UTC, i.e.  $u_{\text{O}}$  is not sufficiently correlated with  $u_{\text{AWS}}$  at these times for the additional variability of  $u_{\text{O}}$  to produce a reduction in mean square error. Thus, while the bias between Official and AWS is lower, or about the same, as that between ECMWF and AWS, the higher random variability of Official results in higher mean square error for most of the day. Figure 16 shows similar conclusions can be drawn for the meridional perturbations at Darwin Airport, although in this case  $\text{var}(u_{\text{O}}) > \text{var}(u_{\text{E}})$

561 for the entire day. Most of the difference between the WPI and CWPI scores for the Official ver-  
562 sus ECMWF comparison at Darwin Airport in Figures 6 and 10, respectively, can be explained  
563 through the different mean square error and bias terms for the zonal perturbations alone.

564 Figure 14 a) shows that ECMWF’s climatological perturbations at Darwin Airport underestimate  
565 the easterly perturbations from 00:00 to 03:00 UTC, which are presumably associated with bound-  
566 ary layer mixing processes. Official does a better job of resolving these easterly perturbations, but  
567 is generally outperformed by ECMWF in resolving the northerly sea-breeze perturbations. Similar  
568 points can be made for the Darwin and NT coastal station groups. While spatial averaging reduces  
569 a portion of the unpredictable variability in Official, Official also often has larger meridional biases  
570 at these scales compared to ECMWF. Figures 14 and 12 show that these biases can be explained  
571 in terms of amplitude and orientation differences between Official, ECMWF and AWS. Figures  
572 analogous to Figs. 15 and 16, but for other locations around Australia, show similar results, but  
573 generally without large biases in the Official forecast at the coarser scales like those present in the  
574 meridional perturbations over the Darwin Airport station group and NT coastal station group.

575 These examples illustrate the idea that the additional unpredictable variability introduced by a  
576 higher resolution edited forecast needs to be “paid for” by a reduction in bias, otherwise the net  
577 result will just be an increase in error. One obvious way to reduce the influence of unpredictable  
578 variability at higher resolutions is to move to an ensemble forecasting approach. However, compu-  
579 tational resources typically require a choice between either a single model of higher resolution, or  
580 an ensemble of models at lower resolution, and there is a long and spirited debate in the literature  
581 about the relative merits of each (Brooks and Doswell III 1993). If ensemble forecasting is not  
582 possible, careful thought must be given to precisely what scales of motion the Official forecast is  
583 intended to represent. If the end user doesn’t care about the “realism” of the forecast and simply  
584 wants the lowest errors, and if daily errors are larger with a higher resolution, edited forecast,

585 than with a coarse model guidance product, there may be an argument for smoothing or filtering  
586 the higher resolution forecast before it is provided to the end user, assuming of course the higher  
587 resolution forecast actually reduces biases.

588 Furthermore, it is unclear if the Official forecast's wind fields are intended to be regarded as  
589 predictions of the actual winds at a specific location, or a predicted Reynold's average, and if so,  
590 at what scale. If we assume the BoM's Official wind forecast intends to represent variability at  
591 hourly timescales, and horizontal scales less than 50 kms, then sea-breeze and boundary layer  
592 mixing edits appear to have little effect, because the intended reduction in error is washed out by  
593 the unpredictable turbulent variability at these scales, and lower errors can be achieved simply by  
594 using a coarser resolution unedited model forecast. However, some users may be more interested  
595 in whether the variability of the forecast wind field matches those of observations, than in whether  
596 the forecast minimises absolute error, and a higher resolution edited forecast will likely perform  
597 better than a coarse resolution model in this regard.

598 Ambiguity in what the Official forecast represents, and the resulting verification challenge,  
599 points to an important role for human forecasters: post-processing and editing model data so  
600 that the forecast consistently represents what is of interest to individual users. One barrier to this  
601 is that the Official forecast is provided to the national public as a whole, which includes diverse  
602 users with different representation needs. Part of the solution may therefore be the development  
603 of a secondary economy, either within national weather services like the BoM, or in the private  
604 sector, where human forecasters ensure their forecast products consistently represent the "filtered  
605 version of reality" of interest to the end user. This would then help address the representation  
606 problem as it applies to the verification of operational forecasts, as the individual user's represen-  
607 tation needs could then be taken as the intended representation of the forecast, and appropriate  
608 verification metrics chosen accordingly.

## 5. Conclusion

In this paper we have presented a method for verifying the diurnal component of wind forecasts issued to the public, with the intended application being the assessment of the edits Australian forecasters make to model guidance datasets in order to better resolve land-sea breeze and boundary layer mixing processes. We considered two temporal scales, and three spatial scales, but the method is immediately generalisable to other scales.

When the method is applied to Australian forecast data, the results indicate that when the Official, edited forecast, is assessed on a daily basis, it only produces lower absolute errors in the diurnal wind cycle at very coarse spatial scales of at least 500 km. Even at these scales, the improvements are isolated to particular times of day, and only apply at some locations. Furthermore, while the Official forecast can outperform the two most commonly used model guidance products ACCESS and ECMWF in the sense of absolute error, it rarely outperforms both simultaneously, suggesting that forecaster skill lies more in making the choice of model guidance than in making edits. When the Official forecast is assessed on a seasonal basis, i.e. the average or climatological diurnal wind cycle is assessed, the Official forecast performs better than when assessed on a daily basis, particularly at the single station spatial scale. However, its performance is not overwhelming, as it struggles to unambiguously produce lower absolute error than ACCESS.

An alternative to calculating absolute errors is to assess the realism of structural features of the atmosphere, and following Gille et al. (2005), we do this in an objective way by fitting ellipses to hodographs of the climatological diurnal wind cycles, and deriving structural metrics from the ellipses. In the Australian context this approach reveals structural biases in the Official forecast, including directional biases in the approach of the sea-breeze at Brisbane airport, eccentricity biases along the coast of NSW, and amplitude biases along the southwest coast of WA.

632 Future research could extend this study in multiple directions. An important goal would be to  
633 identify precisely the spatial scale at which the Official forecast can produce lower absolute error  
634 on a daily basis than a coarse model like ECMWF: for Australia over the time period considered,  
635 our study shows that this occurs somewhere between our airport station group scale (50 - 200  
636 km), and coastal station group scale (1000 - 2000 km). Another interesting question is whether the  
637 diurnal component of the Official forecast can outperform a climatological diurnal cycle calculated  
638 from previous observations.

639 In summary, we have shown that forecaster edits can reduce errors in the diurnal cycle of sur-  
640 face winds, but only at very large spatial scales, or in a climatological sense. This scale sensitivity  
641 suggests careful thought needs to be given to how the representation problem applies to the verifi-  
642 cation of operational forecasts. A consistent answer may prove challenging for national forecasting  
643 centres to reach, due to the diverse representation needs of forecast users, and in the Australian  
644 context, due to the hybrid nature of the Official forecast.

645 *Acknowledgments.* Funding for this study was provided for Ewan Short by the Australian Re-  
646 search Council's Centre of Excellence for Climate Extremes (CE170100023). Datasets and soft-  
647 ware were generously provided by the Australian Bureau of Meteorology's Evidence Tasked Au-  
648 tomation team. (Link to Jive homepage or GitHub page? Thanks are due to Michael Foley for  
649 providing support at the Bureau of Meteorology's Melbourne office, and to Craig Bishop for some  
650 helpful conversations. The code written for this study is freely available online (Short 2019).

## 651 **References**

652 Abkar, M., A. Sharifi, and F. Porté-Agel, 2016: Wake flow in a wind farm during a diurnal cycle.  
653 *Journal of Turbulence*, **17** (4), 420–441, doi:10.1080/14685248.2015.1127379.

654 Brooks, H. E., and C. A. Doswell III, 1993: New technology and numerical weather prediction —  
 655 a wasted opportunity? *Weather*, **48** (6), 173–177, doi:10.1002/j.1477-8696.1993.tb05877.x.

656 Bureau of Meteorology, 2010: Operational implementation of the ACCESS numerical weather  
 657 prediction systems. Tech. rep., Bureau of Meteorology, Melbourne, Victoria. [Available online  
 658 at <http://www.bom.gov.au/australia/charts/bulletins/apob83.pdf>].

659 Bureau of Meteorology, 2019: Meteye. Bureau of Meteorology, [Available online at [http://www.](http://www.bom.gov.au/australia/meteye/)  
 660 [bom.gov.au/australia/meteye/](http://www.bom.gov.au/australia/meteye/)].

661 Dai, A., and C. Deser, 1999: Diurnal and semidiurnal variations in global surface wind  
 662 and divergence fields. *Journal of Geophysical Research*, **104**, 31 109–31 125, doi:10.1029/  
 663 1999JD900927.

664 Ebert, E. E., 2008: Fuzzy verification of high-resolution gridded forecasts: a review and proposed  
 665 framework. *Meteor. Appl.*, **15** (1), 51–64, doi:10.1002/met.25.

666 Efron, B., 1979: Bootstrap methods: Another look at the jackknife. *The Annals of Statistics*, **7** (1),  
 667 1–26, doi:10.1214/aos/1176344552.

668 Englberger, A., and A. Dörnbrack, 2018: Impact of the diurnal cycle of the atmospheric bound-  
 669 ary layer on wind-turbine wakes: a numerical modelling study. *Boundary-Layer Meteorology*,  
 670 **166** (3), 423–448, doi:10.1007/s10546-017-0309-3.

671 European Center for Medium Range Weather Forecasting, 2018: *Part IV: Physical processes*.  
 672 No. 4, IFS Documentation, European Center for Medium Range Weather Forecasting, [Avail-  
 673 able online at <https://www.ecmwf.int/node/18714>].

674 Gille, S. T., S. G. Llewellyn Smith, and N. M. Statom, 2005: Global observations of the land  
 675 breeze. *Geophysical Research Letters*, **32** (5), doi:10.1029/2004GL022139.

Griffiths, D., H. Jack, M. Foley, I. Ioannou, and M. Liu, 2017: Advice for automation of forecasts: a framework. Tech. rep., Bureau of Meteorology, Melbourne, Victoria. [Available online at <http://www.bom.gov.au/research/publications/researchreports/BRR-021.pdf>].

Lee, X., 2018: *Fundamentals of boundary-layer meteorology*. Springer atmospheric sciences, Springer.

Lock, A. P., A. R. Brown, M. R. Bush, G. M. Martin, and R. N. B. Smith, 2000: A new boundary layer mixing scheme. Part I: scheme description and single-column model tests. *Monthly Weather Review*, **128** (9), 3187–3199, doi:10.1175/1520-0493(2000)128<3187:ANBLMS>2.0.CO;2.

Louis, J.-F., 1979: A parametric model of vertical eddy fluxes in the atmosphere. *Boundary-Layer Meteorology*, **17** (2), 187–202, doi:10.1007/BF00117978.

Lynch, K. J., D. J. Brayshaw, and A. Charlton-Perez, 2014: Verification of European sub-seasonal wind speed forecasts. *Monthly Weather Review*, **142** (8), 2978–2990, doi:10.1175/MWR-D-13-00341.1.

Mass, C. F., D. Ovens, K. Westrick, and B. A. Colle, 2002: Does increasing horizontal resolution produce more skillful forecasts? *Bulletin of the American Meteorological Society*, **83** (3), 407–430, doi:10.1175/1520-0477(2002)083<0407:DIHRPM>2.3.CO;2.

Miller, S. T. K., B. D. Keim, R. W. Talbot, and H. Mao, 2003: Sea breeze: Structure, forecasting, and impacts. *Reviews of Geophysics*, **41** (3), doi:10.1029/2003RG000124.

Physick, W. L., and D. J. Abbs, 1992: Flow and plume dispersion in a coastal valley. *Journal of Applied Meteorology*, **31** (1), 64–73, doi:10.1175/1520-0450(1992)031<0064:FAPDIA>2.0.CO;2.

Pinson, P., and R. Hagedorn, 2012: Verification of the ECMWF ensemble forecasts of wind speed against analyses and observations. *Meteor. Appl.*, **19** (4), 484–500, doi:10.1002/met.283.

Rife, D. L., and C. A. Davis, 2005: Verification of temporal variations in mesoscale numerical wind forecasts. *Monthly Weather Review*, **133** (11), 3368–3381, doi:10.1175/MWR3052.1.

SciPy, 2019: Optimization and root finding (scipy.optimize). SciPy, [Available online at <https://docs.scipy.org/doc/scipy/reference/optimize.html>].

Short, E., 2019: eshort0401/forecast\_verification\_paper. GitHub, [Available online at [https://github.com/eshort0401/forecast\\_verification\\_paper](https://github.com/eshort0401/forecast_verification_paper)].

Svensson, G., and Coauthors, 2011: Evaluation of the diurnal cycle in the atmospheric boundary layer over land as represented by a variety of single-column models: The second GABLS experiment. *Boundary-Layer Meteorology*, **140** (2), 177–206, doi:10.1007/s10546-011-9611-7.

Vincent, C. L., and T. P. Lane, 2016: Evolution of the diurnal precipitation cycle with the passage of a Madden–Julian Oscillation event through the Maritime Continent. *Monthly Weather Review*, **144** (5), 1983–2005, doi:10.1175/MWR-D-15-0326.1.

Wilks, D. S., 2011: *Statistical methods in the atmospheric sciences*. International geophysics series: v. 100, Elsevier.

Zaron, E. D., and G. D. Egbert, 2006: Estimating open-ocean barotropic tidal dissipation: The hawaiian ridge. *Journal of Physical Oceanography*, **36** (6), 1019–1035, doi:10.1175/JPO2878.1.

Zwiers, F. W., and H. von Storch, 1995: Taking serial correlation into account in tests of the mean. *Journal of Climate*, **8** (2), 336–351, doi:10.1175/1520-0442(1995)008<0336:TSCIAI>2.0.CO;2.



719 **LIST OF TABLES**

720	<b>Table 1.</b>	Average 10 m wind speeds for austral winter (June, July August) 2018, and	
721		austral summer (December, January, February) 2017/18 across the eight Aus-	
722		tralian capital city airport weather stations. . . . .	34

Airport	Austral Summer	Austral Winter
Darwin	6.3 kn	6.2 kn
Brisbane	8.6 kn	7.0 kn
Perth	11.3 kn	7.9 kn
Sydney	12.2 kn	10.2 kn
Adelaide	9.5 kn	10.3 kn
Canberra	7.4 kn	7.9 kn
Melbourne	10.0 kn	12.1 kn
Hobart	10.0 kn	8.7 kn

723 TABLE 1. Average 10 m wind speeds for austral winter (June, July August) 2018, and austral summer (De-  
724 cember, January, February) 2017/18 across the eight Australian capital city airport weather stations.

## LIST OF FIGURES

<b>Fig. 1.</b>	Locations of the automatic weather stations used in this study. Stars indicate capital city airport stations. Height and depth shading intervals every 200 and 1000 m, respectively. . . . .	37
<b>Fig. 2.</b>	Heatmaps of $\overline{WPI}$ values, a), c), e), and confidence scores, b), d), f), for each coastal station group and hour of the day: Official versus ACCESS, a) and b), Official versus ECMWF, c) and d), ECMWF versus ACCESS, e) and f). Positive $\overline{WPI}$ values indicate that the former dataset in each pair is on average $\overline{WPI}$ kn closer to observations than the latter dataset is. Confidence scores provide the probability the population or “true” value of $\overline{WPI}$ is greater than zero. . . . .	38
<b>Fig. 3.</b>	Time series, a), of $\overline{WPI}_{OA}$ and $\overline{WPI}_{OE}$ for the NT station group at 23:00 UTC, and b), hodographs showing hourly changes in winds, and c), wind perturbations, at the NT station group on the 3 <sup>rd</sup> of July 2018. . . . .	39
<b>Fig. 4.</b>	As in Fig. 3, but for, a), the South WA station group at 05:00 UTC, and b) and c), the winds and wind perturbations over the South WA station group on the 9 <sup>th</sup> June 2018. . . . .	40
<b>Fig. 5.</b>	Wind soundings at, a), Darwin Airport, and b), Perth Airport. . . . .	41
<b>Fig. 6.</b>	The $\overline{WPI}_{OE}$ values, a) and c), and confidence scores, b) and d), for the airport stations, a) and b), and airport station groups, c) and d). . . . .	42
<b>Fig. 7.</b>	As in Fig. 6, but for the $\overline{WPI}_{EA}$ values and confidence scores. . . . .	43
<b>Fig. 8.</b>	As in Fig. 2, but for the CWPI values and confidence scores. . . . .	44
<b>Fig. 9.</b>	Average wind perturbations over June, July and August 2018 for the, a), North WA, b) South WA, c) NSW and d), SA coastal station groups. . . . .	45
<b>Fig. 10.</b>	As in Fig. 6, but for the CWPI values and confidence scores. . . . .	46
<b>Fig. 11.</b>	$R^2$ values as percentages for the fit of equation (5) to the zonal perturbations, a), c) and e), and equation (6) to the meridional perturbations, b), d) and f), for the airport stations, a) and b), airport station groups, c) and d), and coastal station groups, e) and f). . . . .	47
<b>Fig. 12.</b>	Metrics derived from fitting the elliptical equations (5) and (6) to the climatological perturbations: maximum perturbation speed, a), e) and i), eccentricity, b), f) and j), orientation, c), g) and k), and time of maximum perturbation, d), h) and l), for the airport stations, a) to d), airport station groups, e) to h), and coastal station groups, i) to l). . . . .	48
<b>Fig. 13.</b>	Hodographs of the climatological perturbations at Brisbane and Hobart airports, a) and d), and the associated ellipse fits, b) and e). For comparison, c) and f) provide hodographs of the climatological perturbations at Spitfire Channel and Hobart (city), respectively. . . . .	49
<b>Fig. 14.</b>	Hodographs of the climatological perturbations at, a), Darwin Airport, b) the Darwin Airport station group, and c), the NT coastal station group. . . . .	50
<b>Fig. 15.</b>	Mean square error between the ECMWF and AWS zonal perturbations $\overline{(u_{AWS} - u_E)^2}$ decomposed into the total variance $\text{var}(u_{AWS} - u_E)$ and squared bias $(\bar{u}_{AWS} - \bar{u}_E)^2$ terms of equation (8), a), e) and i), and analogously for the mean square error between the Official	

762 and AWS zonal perturbations  $\overline{(u_{\text{AWS}} - u_{\text{O}})^2}$ , b), f) and j). Also, the total variance term  
 763  $\text{var}(u_{\text{AWS}} - u_{\text{E}})$  decomposed into the  $\text{var}(u_{\text{AWS}})$ ,  $\text{var}(u_{\text{E}})$  and  $-2 \cdot \text{covar}(u_{\text{AWS}}, u_{\text{E}})$  terms,  
 764 c), g) and k), and analogously for  $\text{var}(u_{\text{AWS}} - u_{\text{O}})$ , d), h) and l). Decompositions given for  
 765 Darwin Airport, a) to d), the Darwin Airport station group, e) to h), and the NT coastal  
 766 station group, i) to l). . . . . 51

767 **Fig. 16.** As in Fig. 15, but for the meridional perturbations. . . . . 52

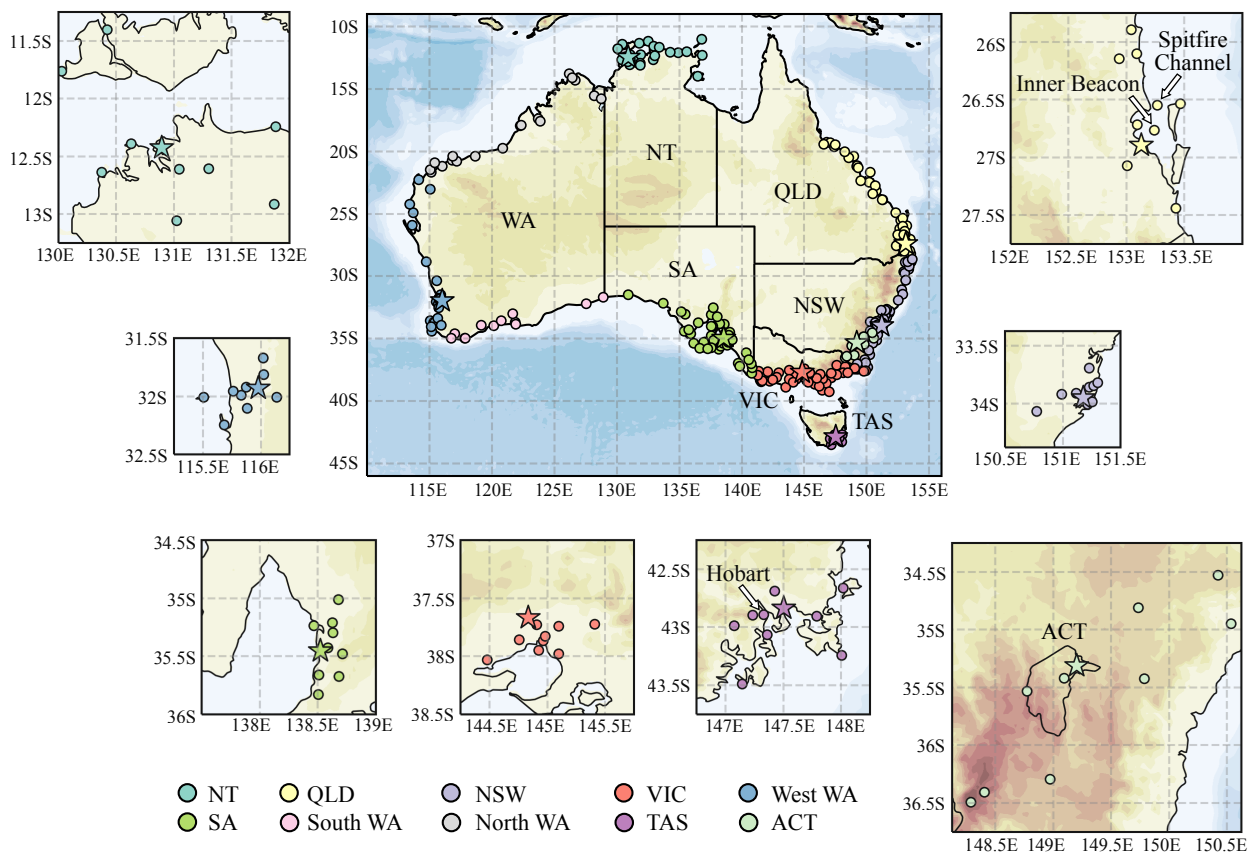


FIG. 1. Locations of the automatic weather stations used in this study. Stars indicate capital city airport stations. Height and depth shading intervals every 200 and 1000 m, respectively.

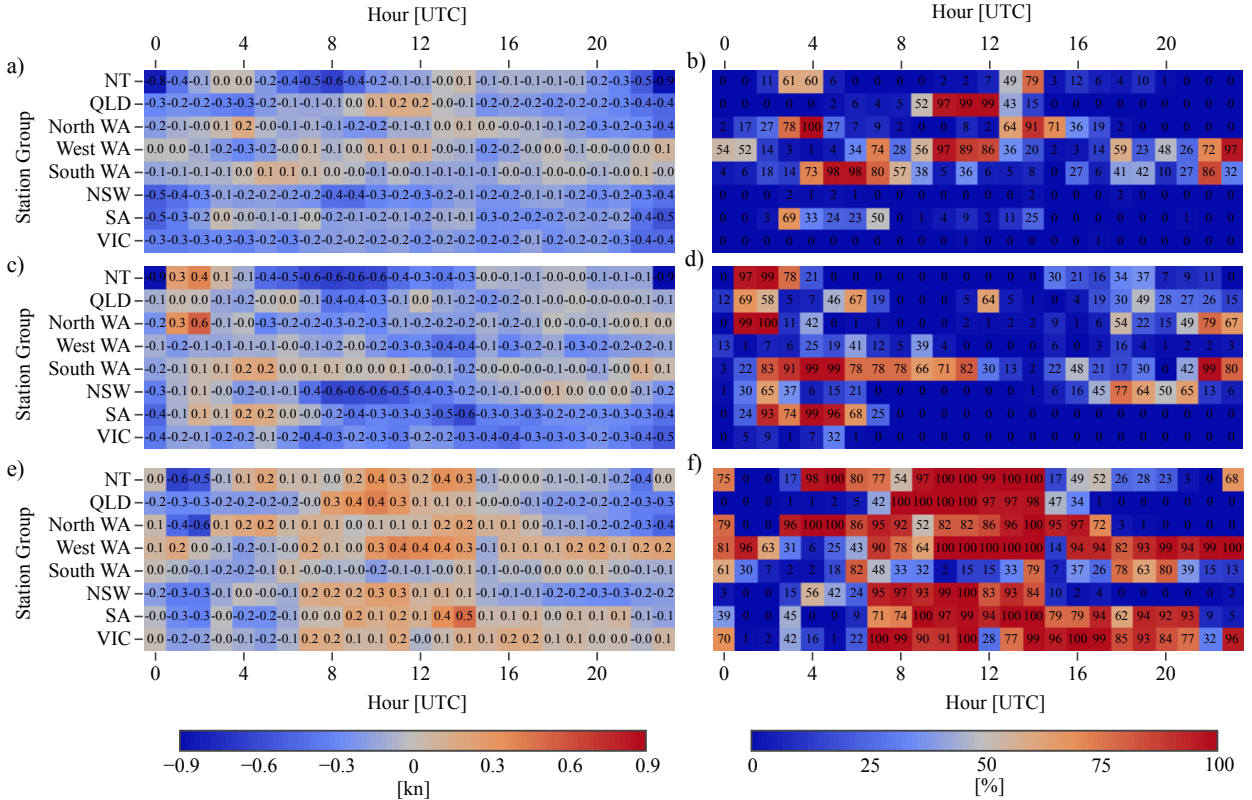


FIG. 2. Heatmaps of  $\overline{\text{WPI}}$  values, a), c), e), and confidence scores, b), d), f), for each coastal station group and hour of the day: Official versus ACCESS, a) and b), Official versus ECMWF, c) and d), ECMWF versus ACCESS, e) and f). Positive  $\overline{\text{WPI}}$  values indicate that the former dataset in each pair is on average  $\overline{\text{WPI}}$  kn closer to observations than the latter dataset is. Confidence scores provide the probability the population or “true” value of  $\overline{\text{WPI}}$  is greater than zero.

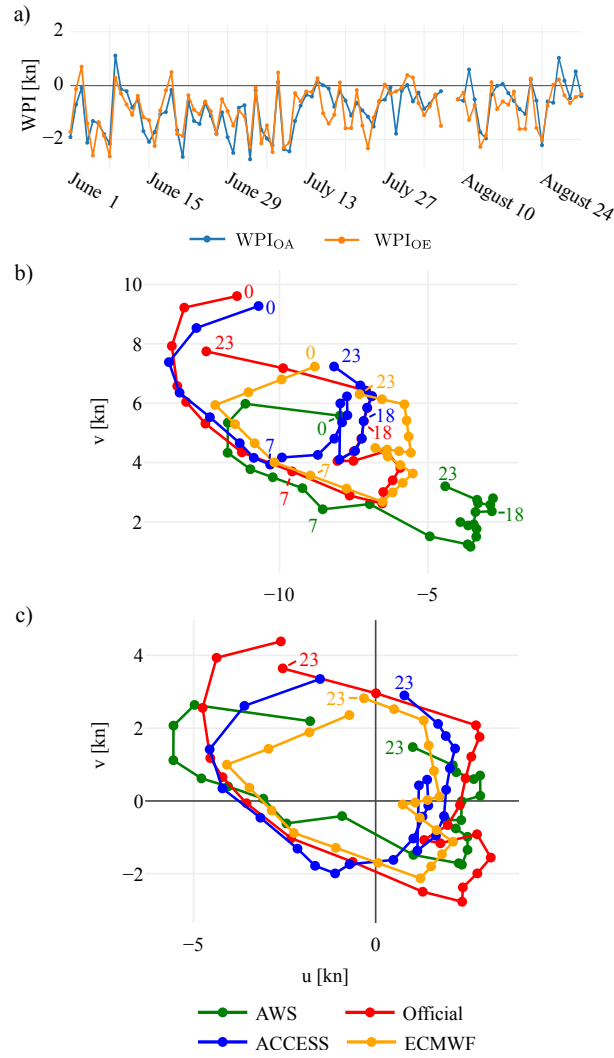


FIG. 3. Time series, a), of  $\overline{WPI}_{OA}$  and  $\overline{WPI}_{OE}$  for the NT station group at 23:00 UTC, and b), hodographs showing hourly changes in winds, and c), wind perturbations, at the NT station group on the 3<sup>rd</sup> of July 2018.

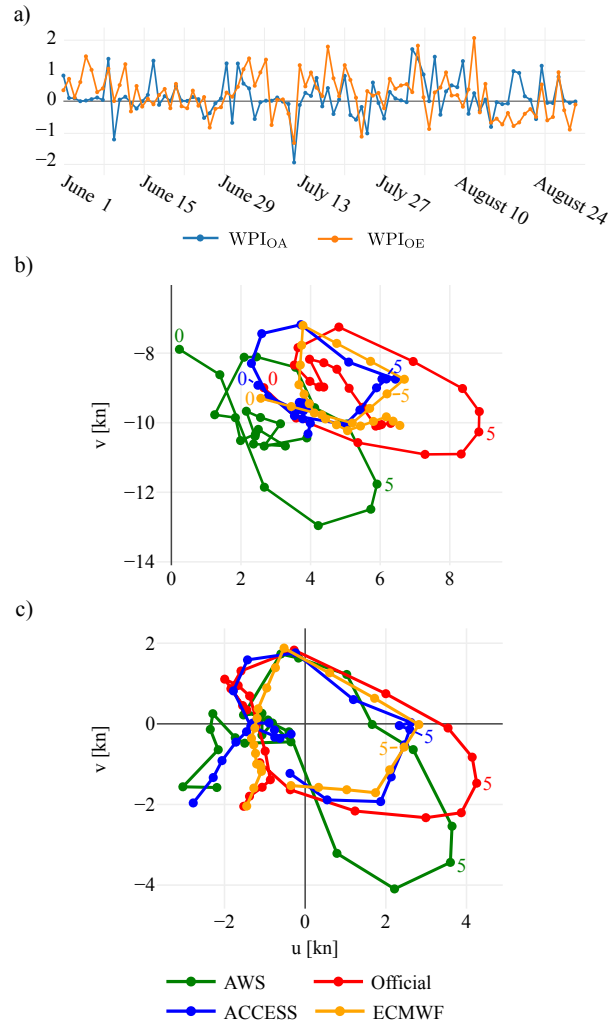


FIG. 4. As in Fig. 3, but for, a), the South WA station group at 05:00 UTC, and b) and c), the winds and wind perturbations over the South WA station group on the 9<sup>th</sup> June 2018.



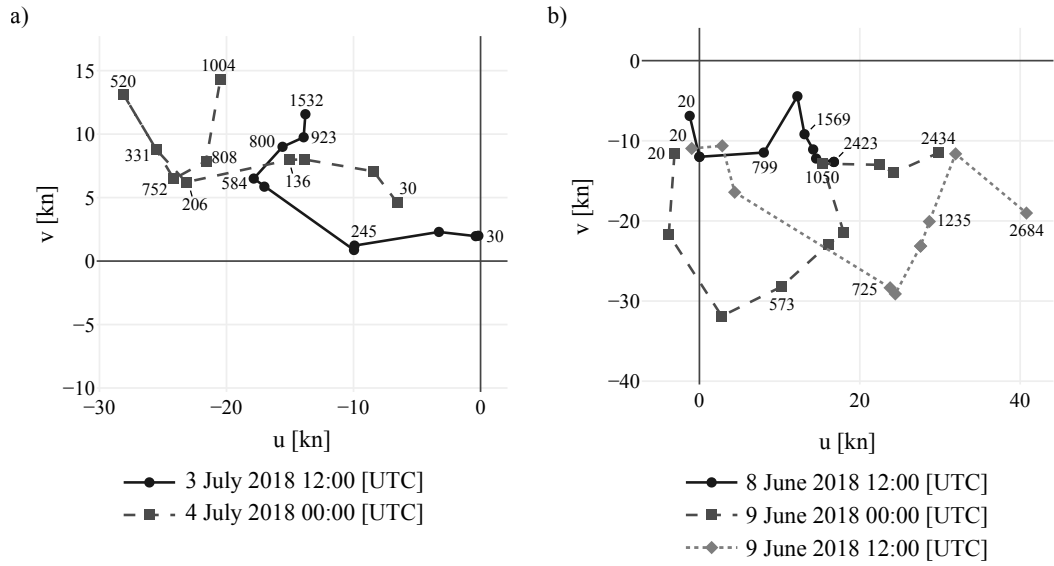


FIG. 5. Wind soundings at, a), Darwin Airport, and b), Perth Airport.

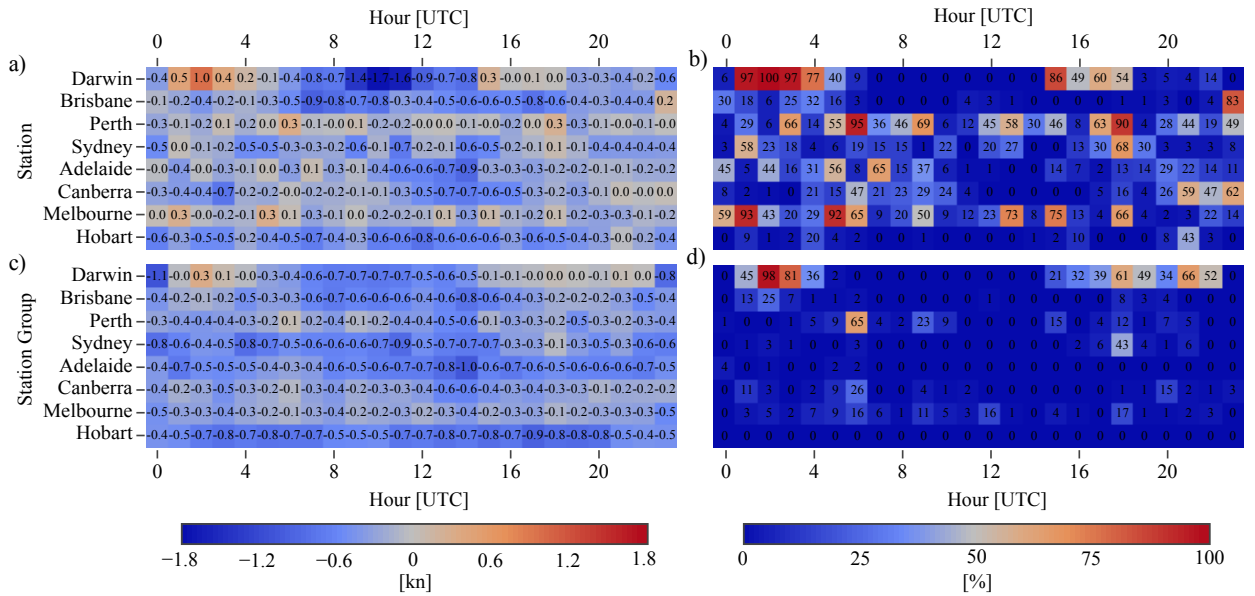


FIG. 6. The  $\overline{\text{WPI}}_{\text{OE}}$  values, a) and c), and confidence scores, b) and d), for the airport stations, a) and b), and airport station groups, c) and d).

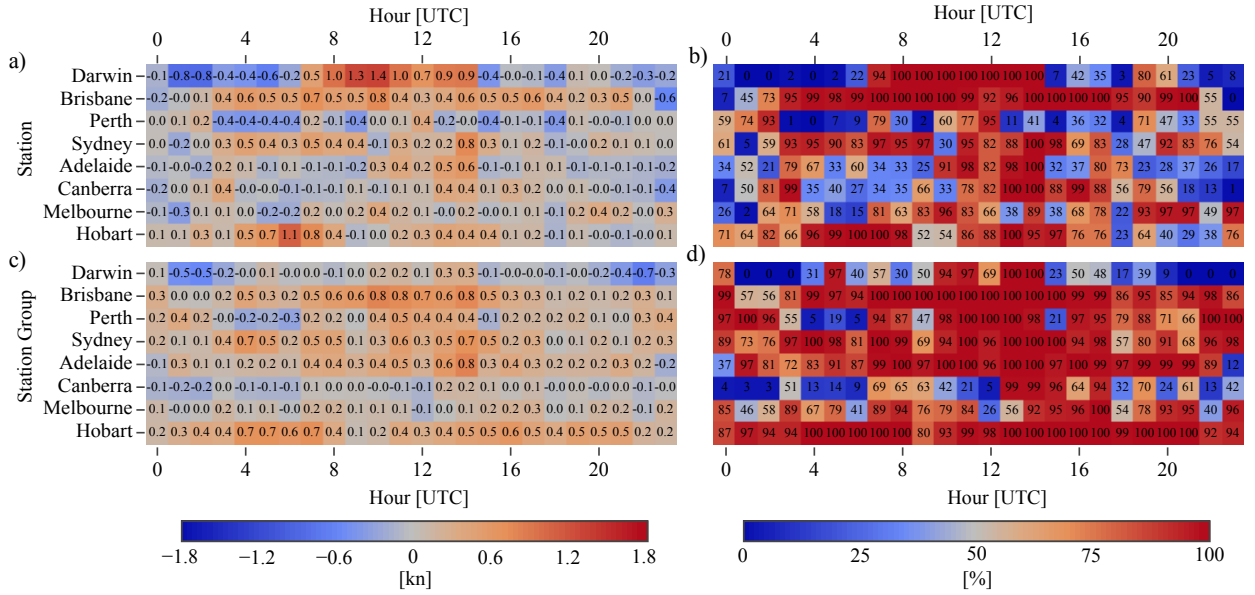


FIG. 7. As in Fig. 6, but for the  $\overline{\text{WPI}}_{\text{EA}}$  values and confidence scores.

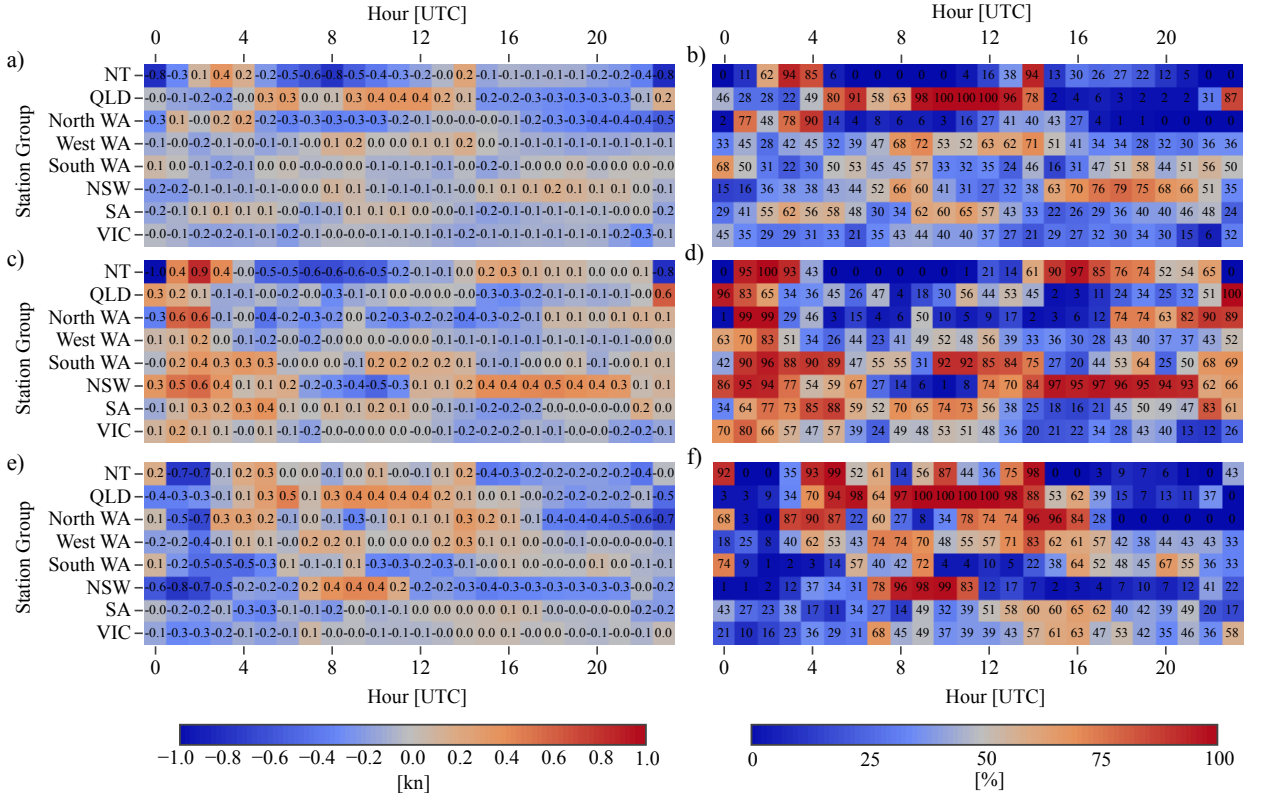
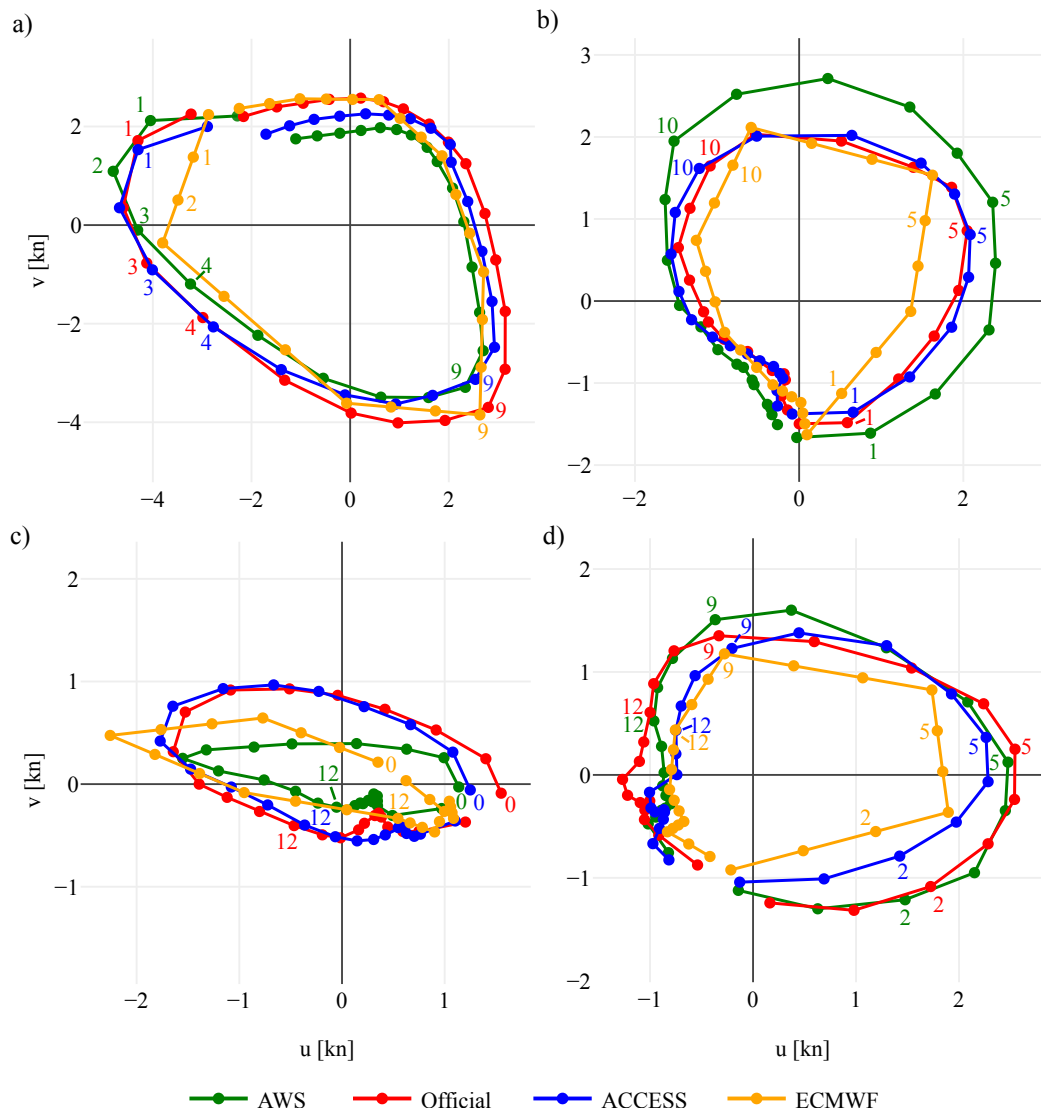


FIG. 8. As in Fig. 2, but for the CWPI values and confidence scores.



781 FIG. 9. Average wind perturbations over June, July and August 2018 for the, a), North WA, b) South WA, c)  
 782 NSW and d), SA coastal station groups.

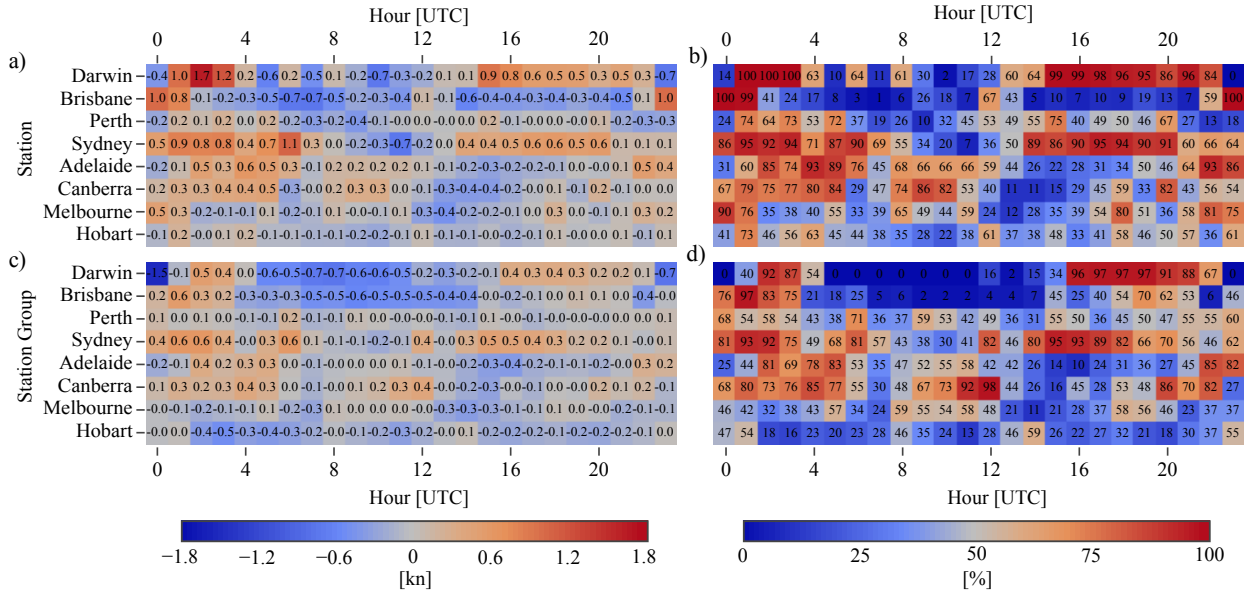


FIG. 10. As in Fig. 6, but for the CWPI values and confidence scores.

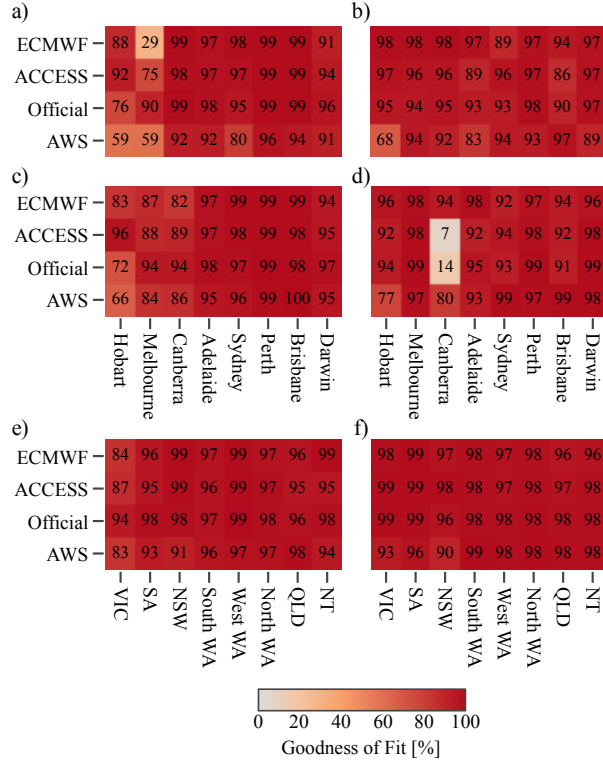


FIG. 11.  $R^2$  values as percentages for the fit of equation (5) to the zonal perturbations, a), c) and e), and equation (6) to the meridional perturbations, b), d) and f), for the airport stations, a) and b), airport station groups, c) and d), and coastal station groups, e) and f).

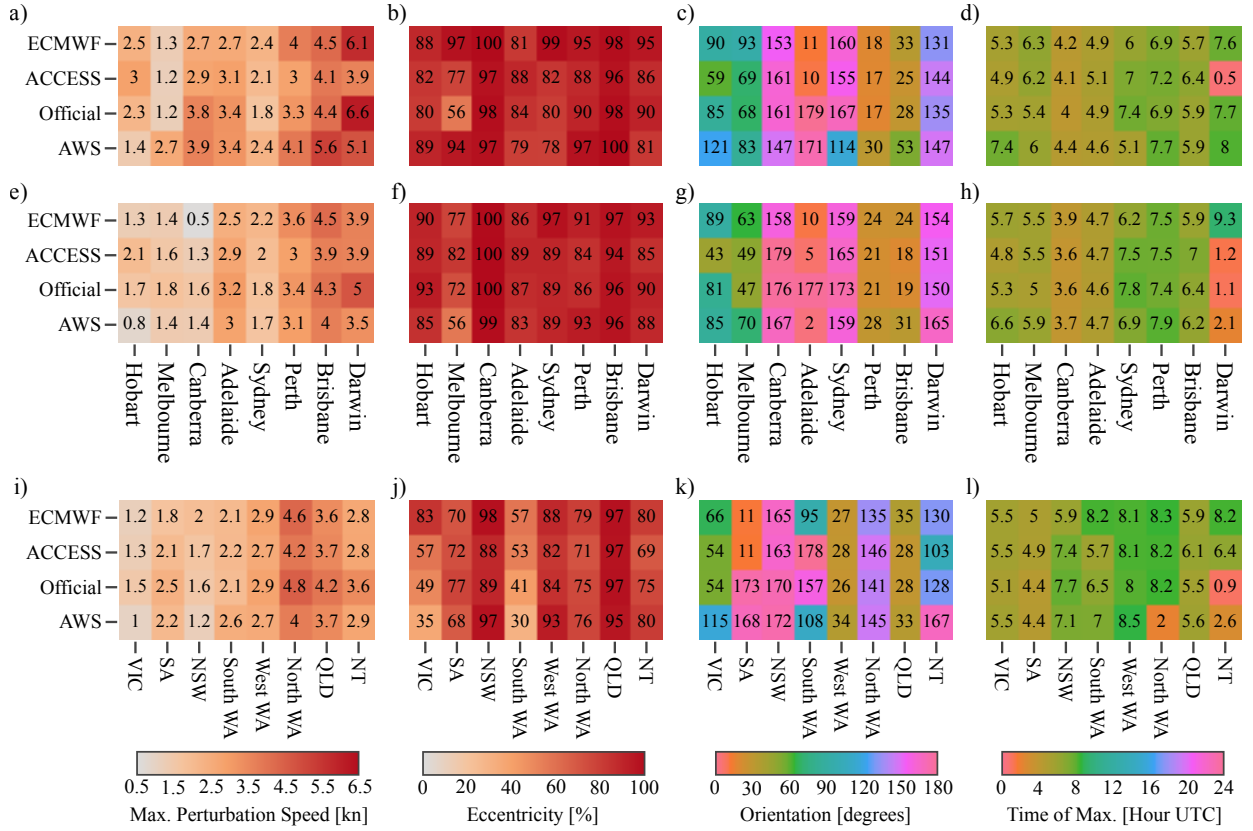


FIG. 12. Metrics derived from fitting the elliptical equations (5) and (6) to the climatological perturbations: maximum perturbation speed, a), e) and i), eccentricity, b), f) and j), orientation, c), g) and k), and time of maximum perturbation, d), h) and l), for the airport stations, a) to d), airport station groups, e) to h), and coastal station groups, i) to l).



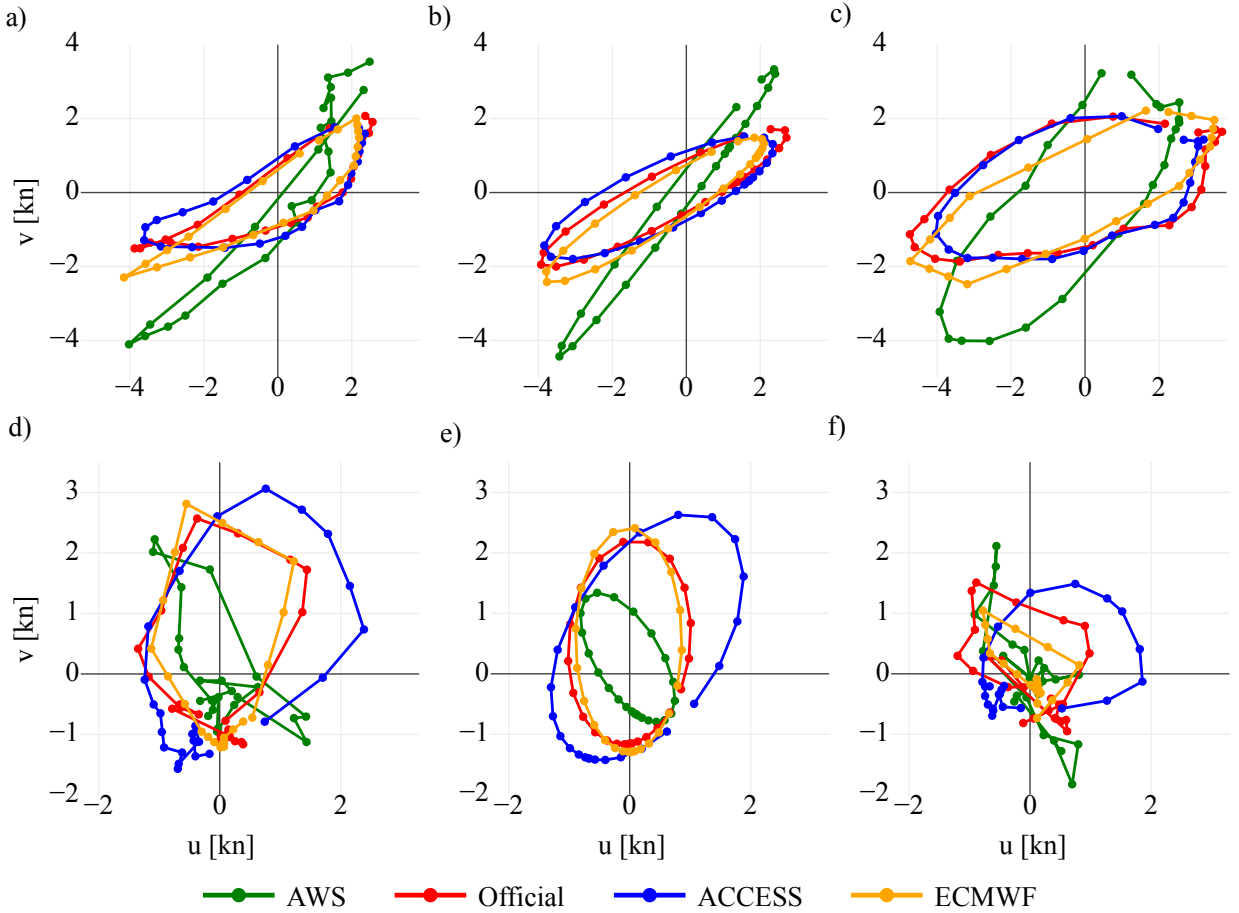
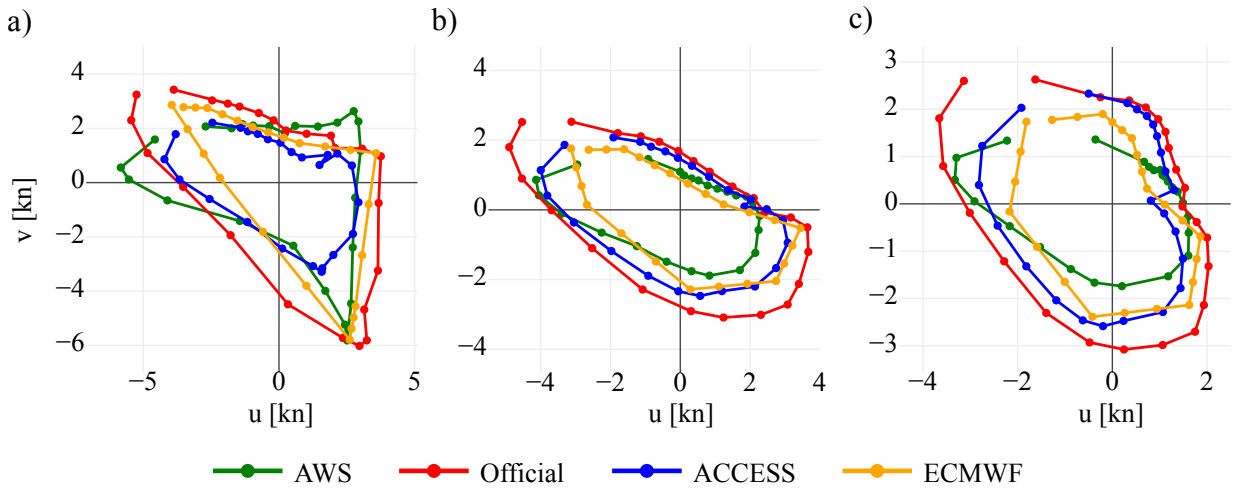


FIG. 13. Hodographs of the climatological perturbations at Brisbane and Hobart airports, a) and d), and the associated ellipse fits, b) and e). For comparison, c) and f) provide hodographs of the climatological perturbations at Spitfire Channel and Hobart (city), respectively.



793 FIG. 14. Hodographs of the climatological perturbations at a), Darwin Airport, b) the Darwin Airport station  
 794 group, and c), the NT coastal station group.

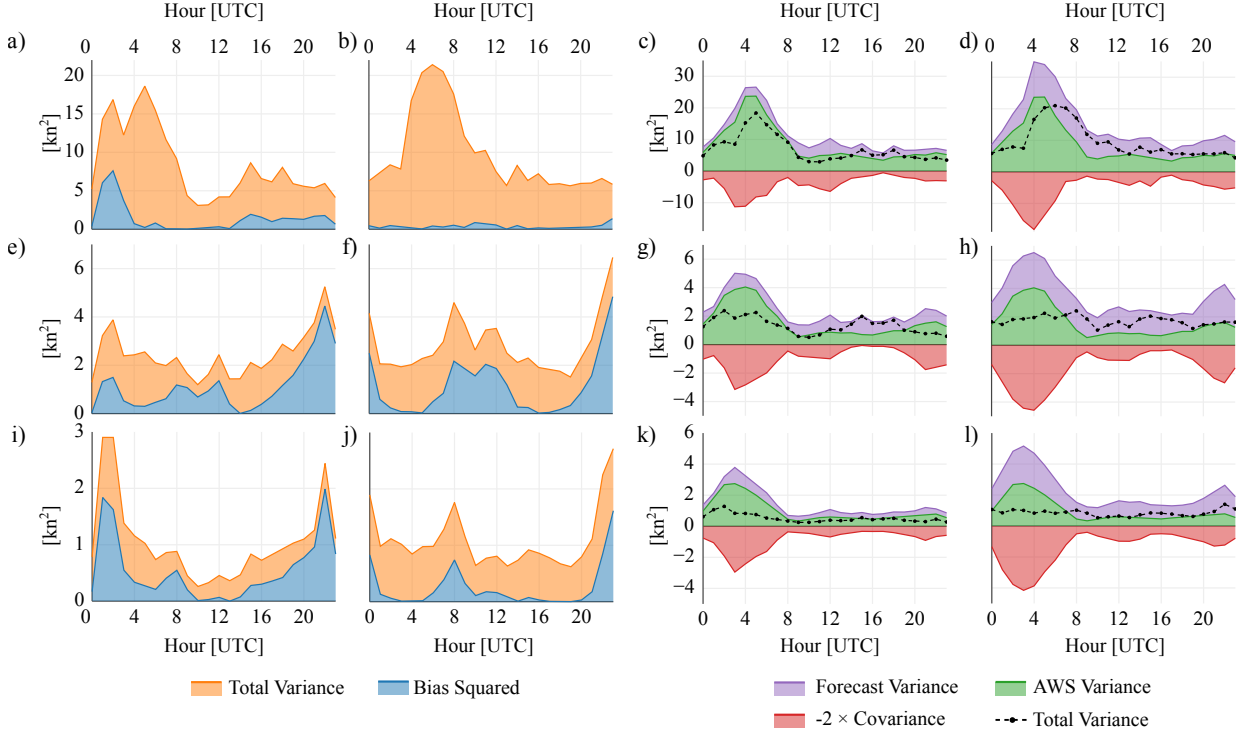


FIG. 15. Mean square error between the ECMWF and AWS zonal perturbations  $\overline{(u_{\text{AWS}} - u_{\text{E}})^2}$  decomposed into the total variance  $\text{var}(u_{\text{AWS}} - u_{\text{E}})$  and squared bias  $(\bar{u}_{\text{AWS}} - \bar{u}_{\text{E}})^2$  terms of equation (8), a), e) and i), and analogously for the mean square error between the Official and AWS zonal perturbations  $\overline{(u_{\text{AWS}} - u_{\text{O}})^2}$ , b), f) and j). Also, the total variance term  $\text{var}(u_{\text{AWS}} - u_{\text{E}})$  decomposed into the  $\text{var}(u_{\text{AWS}})$ ,  $\text{var}(u_{\text{E}})$  and  $-2 \cdot \text{covar}(u_{\text{AWS}}, u_{\text{E}})$  terms, c), g) and k), and analogously for  $\text{var}(u_{\text{AWS}} - u_{\text{O}})$ , d), h) and l). Decompositions given for Darwin Airport, a) to d), the Darwin Airport station group, e) to h), and the NT coastal station group, i) to l).

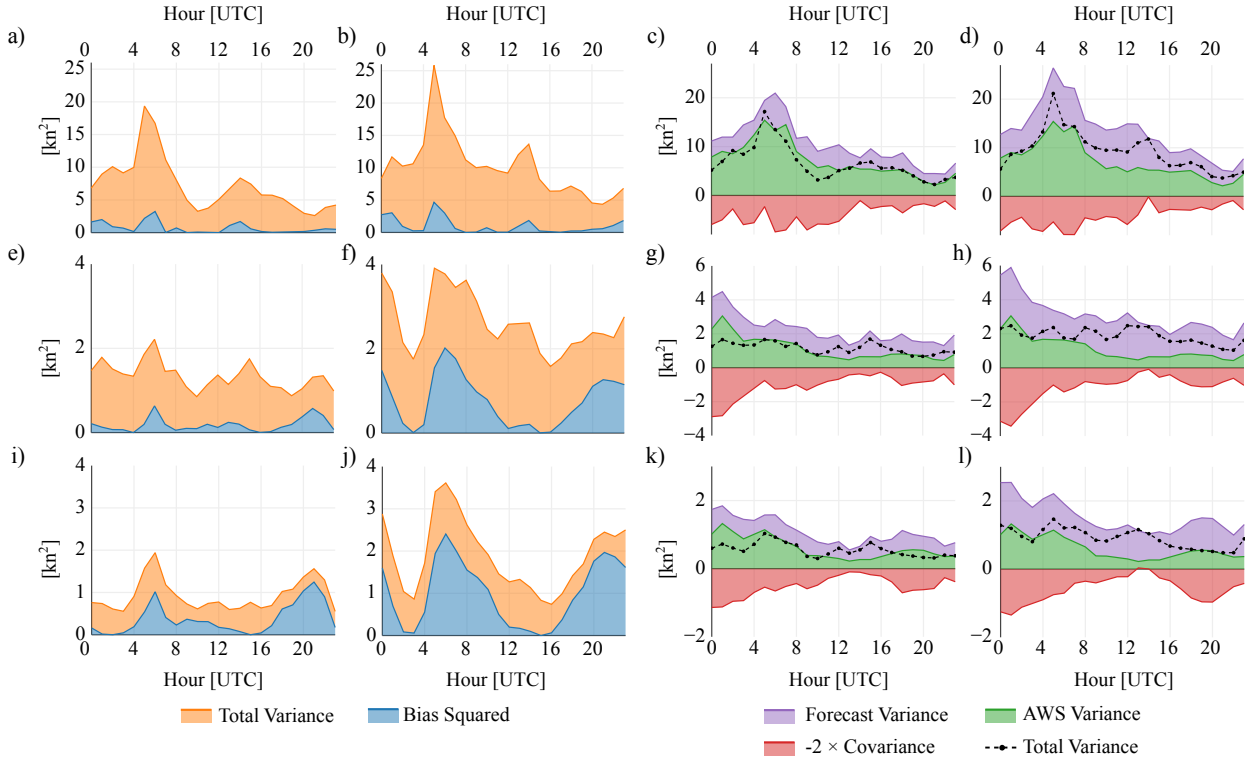


FIG. 16. As in Fig. 15, but for the meridional perturbations.